Meteorol Atmos Phys 93, 53–78 (2006)
DOI 10.1007/s00703-005-0160-9

Meteorology and Atmospheric Physics
Printed in Austria

Department of Mathematical Physics, University College Dublin, Ireland

Simulation of monsoon depressions using MM5: sensitivity to cumulus parameterization schemes

J. Venkata Ratnam* and **E. A. Cox**

With 19 Figures

Received November 4, 2004; revised February 15, 2005; accepted May 21, 2005
Published online: March 15, 2006

Summary

The sensitivity of the simulation of the monsoon depressions to the cumulus parameterization schemes used in a numerical model is studied using the Pennsylvania State University – National Center for Atmospheric Research (PSU-NCAR) model MM5 version 3.6.2. Three different cases of monsoon depressions were studied with a two way interacting domains of 45 km and 15 km resolutions. Two different cumulus parameterization schemes namely Grell (GR) and Kain-Fritsch (KF) were used for the sensitivity study. The model was integrated for 48 hours with the initial and boundary conditions of European Center for Medium Range Weather Forecasting Reanalysis (ERA-40) data. The results show that both the schemes are able to simulate the large scale features of the monsoon depressions realistically. However, both the schemes failed to simulate the exact location of the depression after 24- and 48-hour simulation. The rainfall simulations of both the schemes were very different. The model with the GR scheme tends to over predict the rainfall. The KF scheme could simulate the distribution of the rainfall comparable to the observations. The KF scheme could simulate the maximum observed rainfall but due to locational errors of the simulated depression, the location of the maximum rainfall was not exact. It is also seen that the resolution of the model has a positive impact on the rainfall simulation. The GR and KF schemes were able to realistically simulate the apparent heat sources, but the apparent moisture profile simulated with KF scheme was more comparable to the verifying analysis. The root mean square errors of mean sea-level pressure, temperature, zonal wind and meridional wind were smaller for KF simulation compared to the GR simulation.

1. Introduction

Monsoon depressions originate either in situ or are generated over Bay of Bengal due to the redevelopment of westward-propagating residual lows that move across Indochina. These disturbances are associated with a rainfall amounts of 10–20 cm with in a 24-hour period along their track. The features associated with the depressions have been studied by many researchers (Krishnamurti et al, 1975; Daggupatty and Sikka, 1977; Godbole, 1977; Sikka, 1977; Chen and Yoon, 2000; Stano et al, 2002). Godbole (1977) on compositing five depressions, found that the depressions attain maximum wind speeds of 20 m/s to the south and 15 m/s to the north of depression center at 800 hPa. The thermal structure of the depression was found to have a cold core in the lower troposphere and a warm core overlying it at 500 hPa. Most of the rainfall associated with the depressions occurs in the south-west quadrant of the depression (Godbole, 1977; Stano et al, 2002). Stano et al (2002) on

* Permanent affiliation: Center for Development of Advanced Computing, Pune University Campus, Ganeshkhind, Pune-411 007, India.

examining composite structure of the depressions formed in 1999 using the Tropical Rainfall Measuring Mission (TRMM) data, found that most intense precipitation of the depression is located in the south–southwest of the systems center. They also found that most of the rainfall comes from stratiform processes with isolated, intense convective cells embedded within.

The simulation of the depressions and the rainfall associated with them using numerical models is a challenge faced by the researchers. The numerical simulation of the depressions and the rainfall produced by them is found to be highly dependent on the data used to initialize the model, the resolution of the model and on the physical parameterizations used especially the cumulus parameterization schemes. Due to the limitations in the computational power, the global Numerical Weather Prediction (NWP) models are run at a coarse resolution. Regional NWP models with high resolutions are embedded in the General Circulation Models (GCM) to improve the simulation. The regional models are mainly used to improve upon the GCM simulations by adding the regional features, without deviating much from the GCM's large scale features. There have been many attempts to simulate the monsoon depressions using regional models (Vaidya and Singh, 1997, 2000; Potty et al, 2000; Bhowmik, 2003; Vaidya et al, 2004). Vaidya and Singh (2000) found that the simulated monsoon depressions using regional NWP models were sensitive to the cumulus parameterization schemes used in the model. In their earlier study (Vaidya and Singh, 1997) they found that the simulation was highly dependent on the parameters used within a cumulus scheme. They found an improvement in the track of the depression and the rainfall by adjusting some parameters in the cumulus scheme.

The purpose of the present study is to simulate monsoon depressions using the Pennsylvania State University – National Center for Atmospheric Research (PSU-NCAR) MM5 model and to study their sensitivity to the cumulus parameterization schemes. For the purpose of the study we selected three depressions which formed in the Bay of Bengal in the years 1998 and 1999. The depressions of 1999 formed near the head of the Bay of Bengal, which is the climatologically favorable location for the formation of the depression and moved across the monsoon trough. The depression of 1998 formed over northern parts of west-central and adjoining east-central Bay. These cases provide good scenario for the sensitivity studies.

In the following section, the model setup and the data used for the model runs and for the verification of the simulated results are described. In Sect. 3, the results of the model simulations are discussed and finally in Sect. 4, the conclusions of the study are given.

2. The model and data

2.1 The model

Non-hydrostatic Mesoscale model MM5 Version 3.6.2 (Grell et al, 1994), has been used in this study. MM5 is a nested grid point model with terrain following sigma vertical coordinate system. The model uses Arakawa B-grid staggering in the horizontal with the zonal and meridional velocities defined at the dot points and the scalars temperature, relative humidity etc. defined at the cross points. Two cumulus parameterization schemes, namely Grell (GR) (Grell et al, 1994), and Kain-Fritsch (KF) (Kain and Fritsch, 1993) are used in the model to carryout the sensitivity studies. The default parameters of the cumulus parameterization schemes were used in the study. The KF scheme implicitly does not consider non-precipitating clouds. A shallow convection parameterization scheme based on Grell et al (1994) is used along with the KF scheme to handle the

Table 1. Physical parameterization schemes used in the MM5 model

Physics option	Parameterization scheme
Explicit microphysics	Simple ice scheme (Grell et al, 1994)
PBL	Medium Range Forecast Model (Hong and Pan, 1996)
Radiation	Cloud radiation scheme (Grell et al, 1994)
Surface scheme	Five-layer soil-model (Dudhia, 1996)
Cumulus parameterization	Kain-Fritsch (Kain and Fritsch, 1993) Grell (Grell et al, 1994)
Moisture budget	Bucket Soil Moisture Model (Manabe, 1969)

non-precipitating clouds. The other physics used in the model are given in Table 1. Two way interacting non-hydrostatic domains with horizontal resolutions of 45 km and 15 km were used for the study. In the two way interactions, each domain takes information from the parent domain every time step and runs three time steps for each parent time step before feeding back information to the parent domain on the coincident interior points (Dudhia et al, 2005). In this study both the domains were started at the same time and both the domains were provided initial conditions for startup. Twenty eight vertical sigma levels extending from 1000 hPa to 100 hPa were considered, with 25 hPa difference between the levels till 400 hPa and with 50 hPa difference from 400 hPa to 100 hPa, the top of the atmosphere. A time step of 45 and 15 seconds respectively was used for the integrations of the two domains and the radiation routines were called once after every 30 minutes of the model integration. The model was integrated for 48 hours with the output being saved once every 3 hours.

The KF scheme is a one-dimensional entraining/detraining plume model with mass flux conservation. It considers both updrafts and downdrafts with in a parcel. The closure assumption in this scheme is based on the removal of Convective Available Potential Energy (CAPE) in a grid column within an advective time period (Kain and Fritsch, 1993). The convective precipitation in this scheme is computed as a product of precipitation efficiency and the sum of vertical fluxes of vapor and liquid at about 150 hPa above the condensation level (Wang and Seaman, 1997). A detailed description of the scheme can be found in Bougeault and Mascart (2001).

The GR scheme implemented in MM5 is based on the closure assumption of Arakawa and Schubert (1974) scheme. The closure is based on the assumption that the convective clouds stabilize the environment as fast as the non-convective processes destabilize it. This scheme takes into consideration the updrafts and down drafts in a cloud. There is no direct interaction between the cloud and the environmental air except at the top and bottom of the cloud. The precipitation is calculated as $R = I_1 m_b\ (1 - \beta)$, where R is the precipitation, I_1 is the normalized updraft condensation, m_b is the cloud base mass flux of the updraft and $(1 - \beta)$ is the precipitation efficiency. A detailed description of the scheme is presented in Grell et al (1994).

2.2 Data

Three cases of the monsoon depressions formed over the Bay of Bengal are chosen for the study. Two of the depressions formed in the year 1999 and one in 1998. A brief description of the cases (Thapliyal et al, 1999; 2000) and the domains used for the model integration are described below:

Case I: *Deep depression over the Bay of Bengal during 13–15 June 1998*: On the morning of 13th June 1998, a well marked low-pressure area formed over northern parts of the west-central and adjoining east-central Bay of Bengal. It was seen as a depression at 1200 UTC of 13th June. Moving in a westerly direction, it intensified into a deep depression and was located at 1800 UTC of 13th near 17.5° N, 86.0° E. The deep depression crossed the coast between 1300 and 1400 UTC of 14th and weakened into a depression and was seen as a depression till 0300 UTC 15th June. It weakened into a low by the afternoon of 15th June. The initial conditions of 1200 UTC of 13th June, when the system had intensified into a depression, were used for the model integration. The domains of integration for this case are shown in Fig. 1.

Case II: *Deep depression over the Bay of Bengal 27–29 July 1999*: A well-marked low-pressure area formed over the northwest Bay and adjoining the West Bengal coast on 26th evening. It concentrated into a depression at 0300 UTC of 27th. It intensified into a deep depression and lay centered at 1200 UTC of 22nd near 22.0° N, 88.5° E. It crossed West Bengal–Orissa coast in the morning of 28th and lay as a deep depression at 0300 UTC of 28th. It moved in a west–northwesterly direction and weakened into a depression. It weakened into a well-marked low-pressure area in the evening of 29th. The model was integrated using the initial conditions of 0600 UTC of 27th July over the domains shown in Fig. 2.

Case III: *Depression over the northwest Bay of Bengal 6–8 August 1999*: A well marked low-pressure formed over the northwest Bay off north

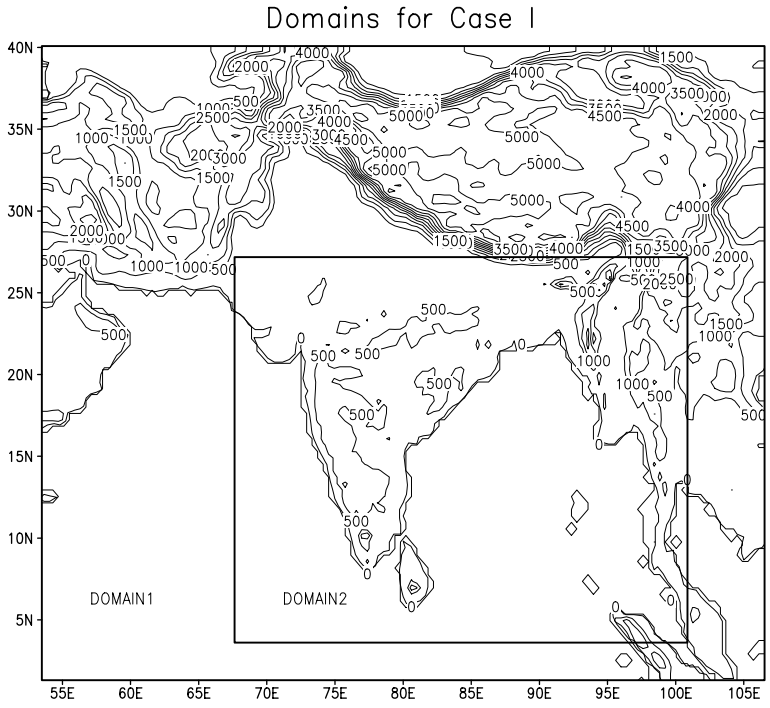

Fig. 1. Domains of integration for Case I. Domain I resolution 45 km, Domain II resolution 15 km

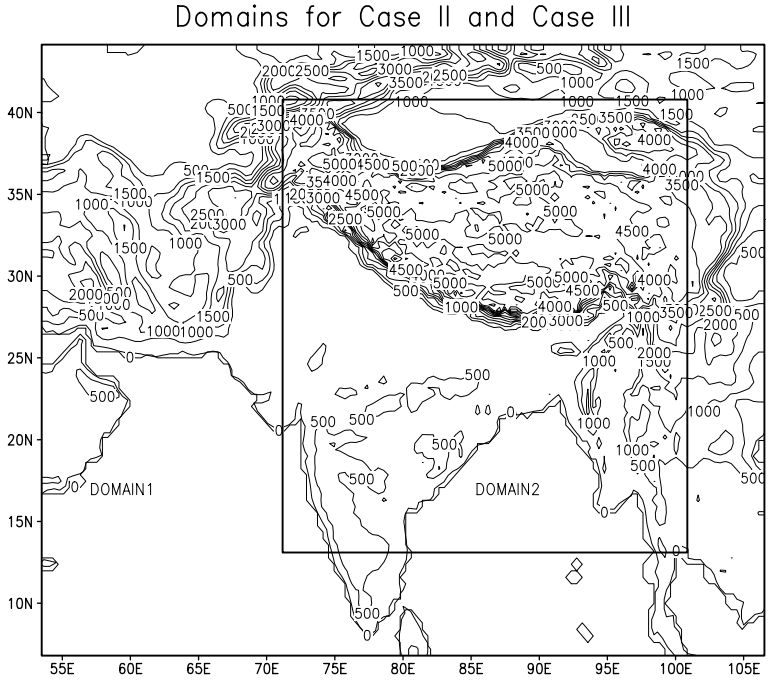

Fig. 2. Same as Fig. 1, but for Case II and Case III

Orissa–West Bengal coast on 6th morning. It concentrated into a depression at 1200 UTC of 6th. It moved in a west–northwesterly direction and crossed West Bengal. It was seen as a depression till 1200 UTC of 8th. It further moved west–northwesterly and weakened into a well-marked low-pressure area on 9th morning. The model integration was from 1200 UTC of 6th August over the domains same as Case II.

The initial and the boundary conditions for both the domains of the model were provided by the six hourly European Center for Medium range Weather Prediction (ECMWF) Reanalysis (ERA-40) data. The post processed ERA-40 data stored at $2.5^\circ \times 2.5^\circ$ Lat./Lon. is used for the studies. The model simulated rainfall is compared with the observed rainfall at nearly 200 stations spread all over India. The observed rain-

fall data was taken from the daily weather reports of India Meteorological Department (IMD). The simulated rainfall over the ocean is compared with the Global Precipitation Climatology Project (GPCP) daily precipitation data. The simulated large-scale atmospheric fields are compared with the ERA-40 data interpolated to the model domain.

3. Results and discussion

3.1 Mean sea-level pressure

The 24- and 48-hour predicted and the corresponding verification Mean Sea-level Pressure (MSLP) fields for the smaller domain with 15 km resolution for Case I are presented in Fig. 3. The results are similar for other cases and also for the larger domain with 45 km resolution, hence the figures are not included. Table 2 gives the central pressure and its location as simulated by the model after 24- and 48-hours of forecast using GR and KF along with ERA-40 MSLP analysis for all the cases. From Fig. 3, it can be seen that for Case I both the schemes were able to simulate the depressions reasonably well. The GR and KF schemes, after 24 hours, simulated depressions deeper than the analysis with central pressures of 1 hpa and 2 hPa less than the verifying analysis. After 48 hours, the KF scheme continued to deepen the depression and a central pressure of 993.1 hPa was simulated, 3 hPa less than the corresponding analysis, whereas the GR scheme simulated a depression of central pressure 1 hPa more than the analysis. However, the distribution of the MSLP over the peninsular and the oceanic regions simulated by the KF scheme was nearer to the analysis compared to the simulations of GR scheme. This feature is seen in all the cases considered for the study (figures not shown). From Table 2, it can be seen GR scheme simulated central pressures of 1 hPa less than the verifying analysis for most of the cases and the KF scheme simulated a central pressures of 2–3 hPa less than the observed MSLP. The locations of the centers of the depressions were reasonably predicted by both the schemes for all the cases after 24 hours of forecast, however large deviations in the locations of the central pressure are seen after 48 hour forecast showing that both the schemes are not able to simulate the tracks of the depressions properly. Godbole (1977) attributed the west–northwestward propagation of the monsoon depressions partly to the pronounced convergence taking place in the north-west sector of a depression and a weak divergence taking place behind the depression. Figure 4 shows the divergence at 850 hPa as simulated by the model after 24- and 36-hours and also the divergence as seen in the ERA-40 data for Case III. From the figure, it can be seen that there is a region of convergence in the north-west sector of the depression and divergence to the east of the depression center, in the ERA-40 data and also in the simulations of the KF and GR after 24-hours of model simulation. By 36 hours of model simulation, both the schemes fail to simulate the convergence in the northwest sector of the depression required for the west–northwestward propagation of the depression. Similar results are seen for Case I and Case II. This partly explains the failure of both the schemes in simulating the track of the depressions properly.

3.2 Wind and temperature

The streamline and isotachs of the wind at 850 hPa for Case I are shown in Fig. 5. From the figure, it can be seen that the ERA-40 winds show a maximum of 15 m/s in the westerly and south westerly flow to the south of the depression center both on 14th and 15th June 1998. Also, it can be seen that the flow is stronger in the southern part of the depression compared to the northern part. The GR scheme simulated winds comparable to reanalysis after 24-hours, with 15 m/s maximum to the south of the depression center. However, the 48 hour forecast winds show a winds of 15 m/s even to the north of the depression center. The KF scheme on the other hand simulated stronger winds of 20 m/s in the southern part after 24 hour forecast and easterlies of the same intensity to the north of the depression center after 48 hours. In Case II (Fig. 6), where the depression was located nearer to the Himalayan region, the 24 hour simulation shows, the winds in the northern part of the depression simulated by both the schemes, having strong easterlies of 10 m/s higher than the reanalysis winds and also stronger than to the south of the depression center. The ERA-40

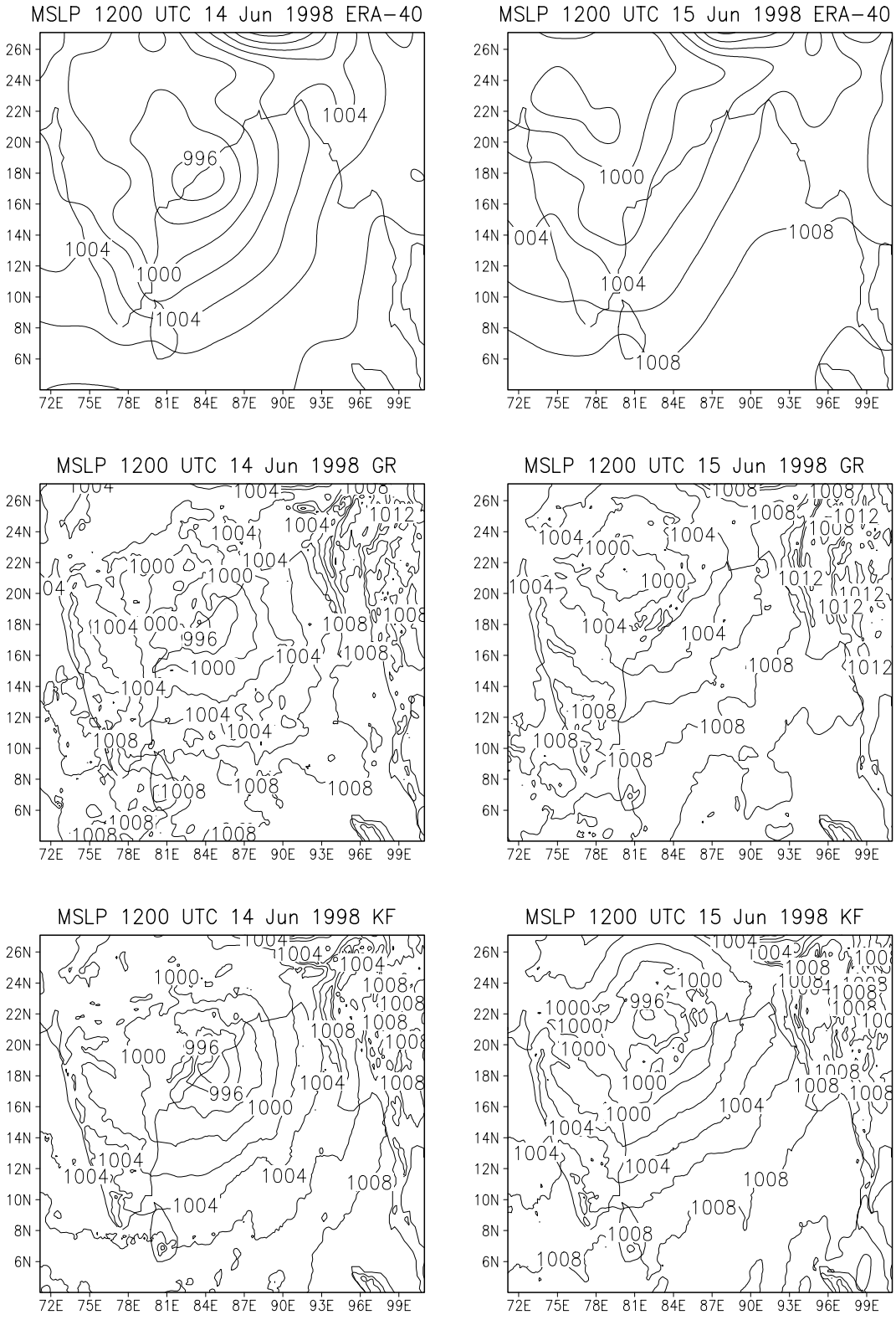

Fig. 3. 24- and 48-hour simulated and the corresponding verification mean sea-level pressure (hPa) for Case I. Domain resolution 15 km, Contour interval 2 hPa. Input: 1200 UTC 13 June 1998. ERA-40 (top), GR (middle) and KF (bottom)

shows the winds to be of similar magnitude of 10 m/s in both the northern and southern parts of the depression. In the case of GR simulations, a spurious cyclonic circulation is seen around the region of 24° N, 81° E on 28th July 1999. This feature is seen even in the larger domain GR

Table 2. Model simulated and corresponding verifying analysis of the central pressure of the monsoon depressions and their locations

	After 24 hr. forecast		After 48 hr. forecast	
	Central pressure (hPa)	Location of the central pressure	Central pressure (hPa)	Location of the central pressure
Case I				
ERA-40	994.75	17.4° N, 83.3° E	996.85	22.9° N, 75.1° E
GR	993.82	18.1° N, 83.4° E	997.96	21.5° N, 80.2° E
KF	992.02	18.2° N, 84.5° E	993.11	21.9° N, 81.8° E
Case II				
ERA-40	994.4	23.6° N, 87.2° E	995.4	25.9° N, 80.3° E
GR	993.9	23.0° N, 87.5° E	994.2	24.7° N, 84.2° E
KF	991.67	23.0° N, 88.6° E	993.2	24.3° N, 83.7° E
Case III				
ERA-40	991.4	24.0° N, 87.2° E	993.1	24.1° N, 83.0° E
GR	989.7	23.2° N, 89.2° E	991.5	22.5° N, 88.3° E
KF	990.7	22.4° N, 87.2° E	989.7	22.6° N, 86.5° E

simulation. In the 48-hour GR simulation, the spurious circulation is not seen, but the pattern of the winds remains similar to Case I, with equal wind speeds in the northern and southern parts of the depression. In Case III (figure not shown), the KF and GR schemes simulated the features similar to Case I.

Figure 7 shows the variation of the zonal and meridional winds with height for the verifying analysis and 24-hour simulations using GR and KF for Case I. The vertical cross sections were constructed using the wind information along the center of the depressions. From the figure it can be seen that, the analysis shows a deep layer of westerlies to the south of the depression center (83.3° E) with a magnitude of 15 m/s. The layer extends from 850 hPa to 550 hPa. The transition from the westerlies to easterlies takes place at about 300 hPa. The easterlies to the north of the depression reach a maximum of 18 m/s at 400 hPa. The zonal wind field is seen to have a slight tilt towards southwest with height. The vertical cross section of the meridional wind field drawn through 17.4° N shows northerlies to the west of the depression reach a maximum peak intensity of 12 m/s at 850 hPa and the southerlies to the east of the depression have a peak of 15 m/s in the layer 925 hPa to 725 hPa and also there is a secondary peak from 525–450 hPa. The vertical cross section of the zonal wind for GR, shows peak westerlies of 18 m/s between 650–600 hPa towards south of the depression and easterlies of 18 m/s to the north of the depression from 900–800 hPa, but the model could not simulate the south west tilt in the vertical. The KF scheme on the other hand was able to simulate the tilt. The KF scheme simulated westerlies of 18 m/s and easterlies on 16 m/s to the south and north of the depression respectively. Both the schemes could simulate the vertical tilt in the meridional wind, but both the schemes simulated northerlies and southerlies of higher magnitude compared to reanalysis. In Case II (Fig. 8), one can see that both the models simulated higher wind speeds compared to the analysis. The spurious cyclonic circulation which was seen in the 850 hPa wind field in the case of GR scheme, can be seen prominently in the vertical cross section of the meridional wind field as southerlies between 81° E – 84° E. This feature is not seen in either the analysis or in the KF simulation. The features similar to Case I are seen in Case III.

The vertical distribution of temperature anomaly, the deviation of temperature from its latitudinal mean, is shown in Figs. 9 and 10. The latitudinal means are calculated at each level for the latitude passing through the center of the depression. The means are calculated over the longitudinal distance of 10°, with the center of the disturbance at the middle of the averaging distance. From Fig. 9, it can be seen that for Case I, the depression has a cold core below 800 hPa at the center of the depression (83.3° E)

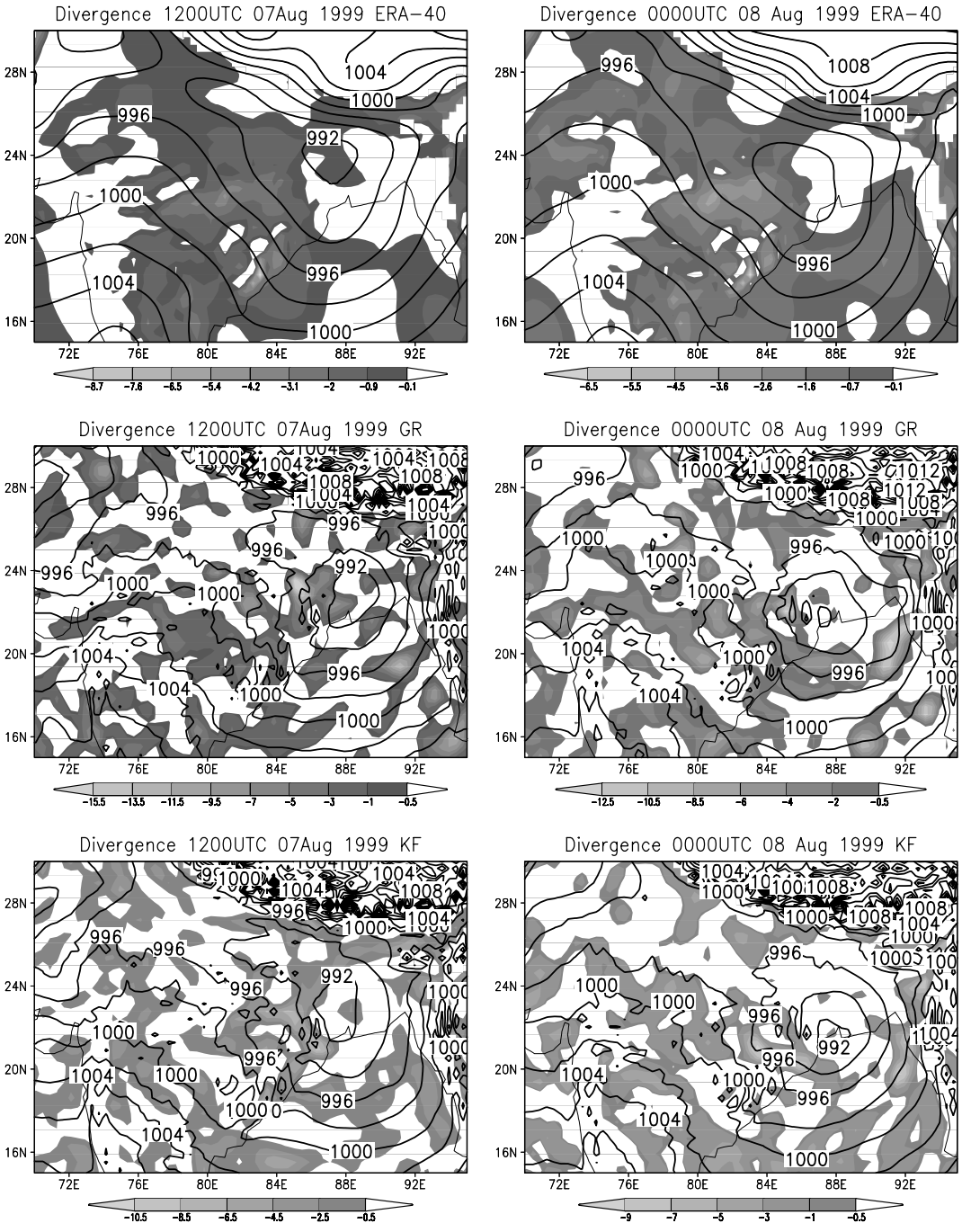

Fig. 4. 24- and 36-hour simulated and the corresponding verification divergence ($\times 10^{-5}\,s^{-1}$) at 850 hPa and isobars (hPa) for Case III. Domain resolution 45 km, Input: 1200 UTC 06 Aug. 1999, ERA-40 (Top), GR (middle) and KF (bottom). Negative divergence is shaded

and a warm core with a maximum of 0.5° K at 300 hPa in the ERA-40 reanalysis. The GR and KF schemes on the other hand simulated a warm core at their centers (83.4° E and 84.5° E, respectively). The warm core is seen up to 450 hPa in case of GR with a peak temperature anomaly of 2.5° K at 700 hPa and is seen throughout the atmosphere in the case of KF scheme with a peak anomaly of 2.0° K at 650 hPa. The GR simulation shows a cold core ahead of the depression and a warm core behind the depression as seen in the ERA-40, but the KF simulation has warm core ahead of the depression. The failure of the GR and KF schemes in simulating the cold core in

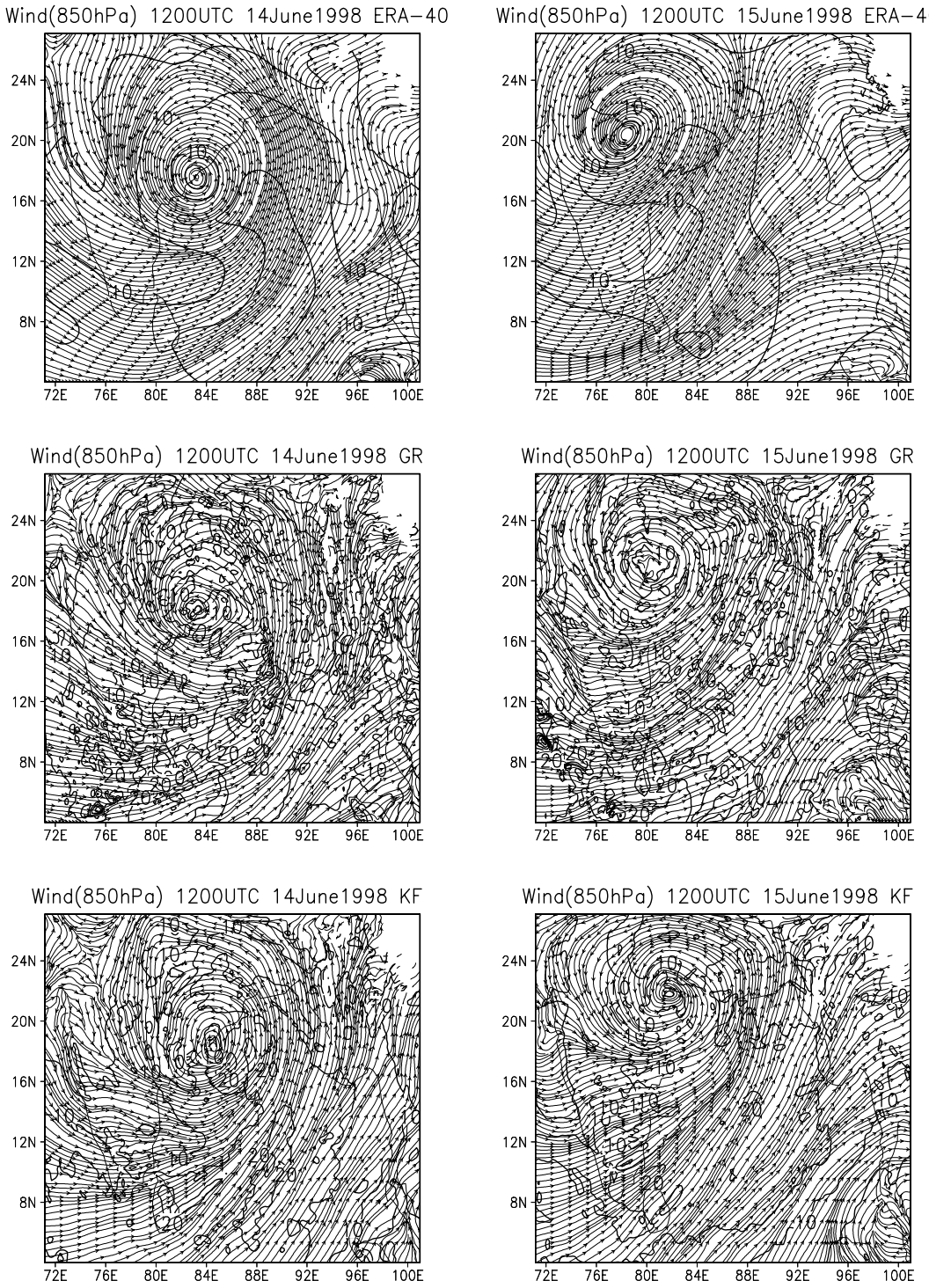

Fig. 5. 24- and 48-hour simulated and the corresponding verification streamlines and isotachs (m/s) for Case I. Domain resolution 15 km, Input: 1200 UTC 13 June 1998, ERA-40 (Top), GR (middle) and KF (bottom)

the lower levels may be because of strong intensity depression simulated by them.

In Case II and Case III, the ERA-40 shows a warm at the center and a cold region ahead of the depression at lower levels. The GR and KF schemes could simulate the warm central core but only GR scheme simulated the cold core ahead of the depression center.

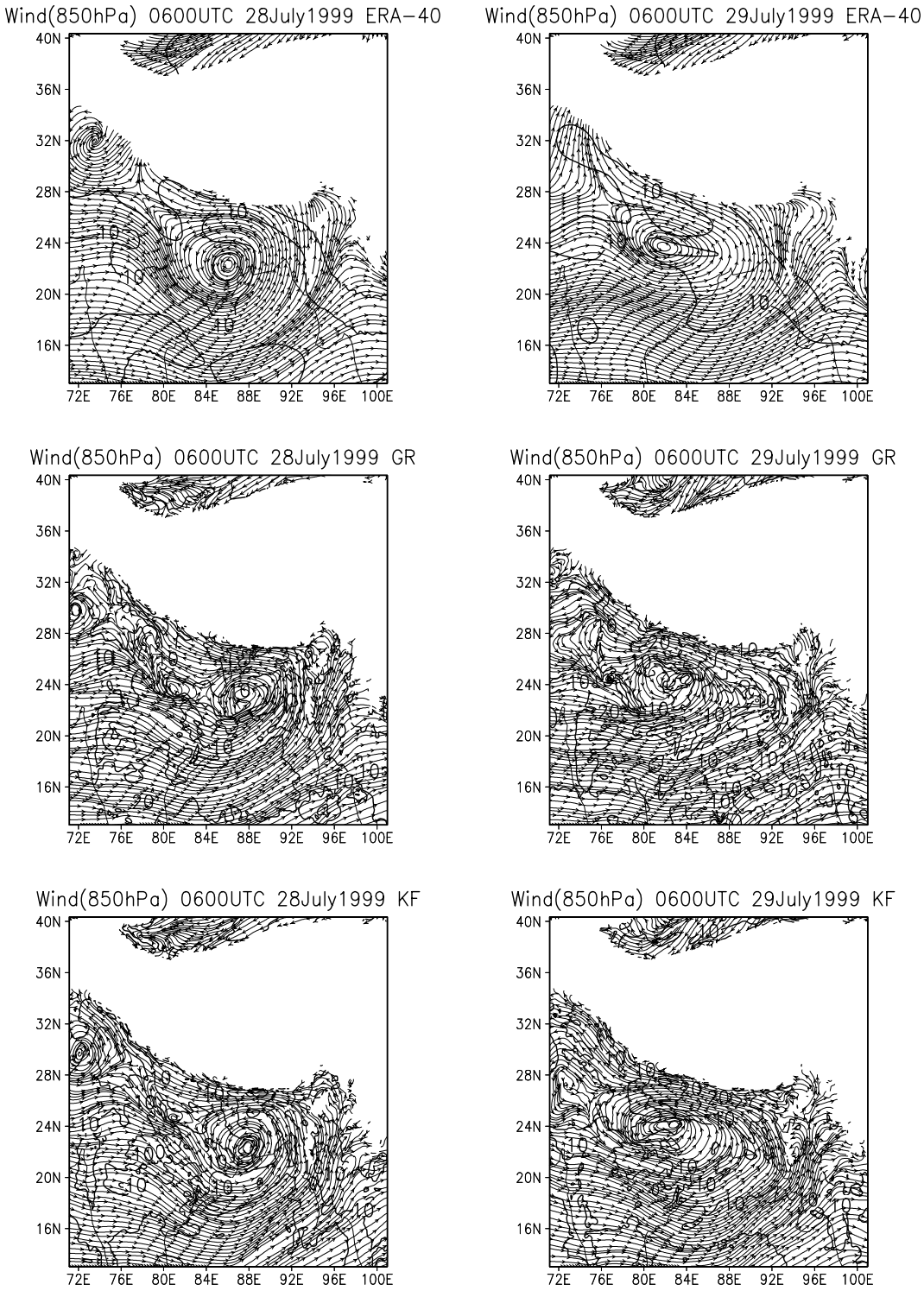

Fig. 6. Same as Fig. 5, but for Case II. Input: 0600 UTC 27 July 1999

3.3 Relative vorticity

The vertical cross sections of the relative vorticity through the center of the depressions is shown in Figs. 11, 12 and 13. From Fig. 11 (Case I), it can be seen that the GR scheme simulated a maximum vorticity of $20 \times 10^{-05}\,s^{-1}$ at 700 hPa and at 850 hPa after 24- and 48-hours, respectively. The KF scheme simulated a vorticity of $20 \times 10^{-05}\,s^{-1}$ at 400 hPa after 24 hours of simulation and after 48 hours a maximum vorticity of

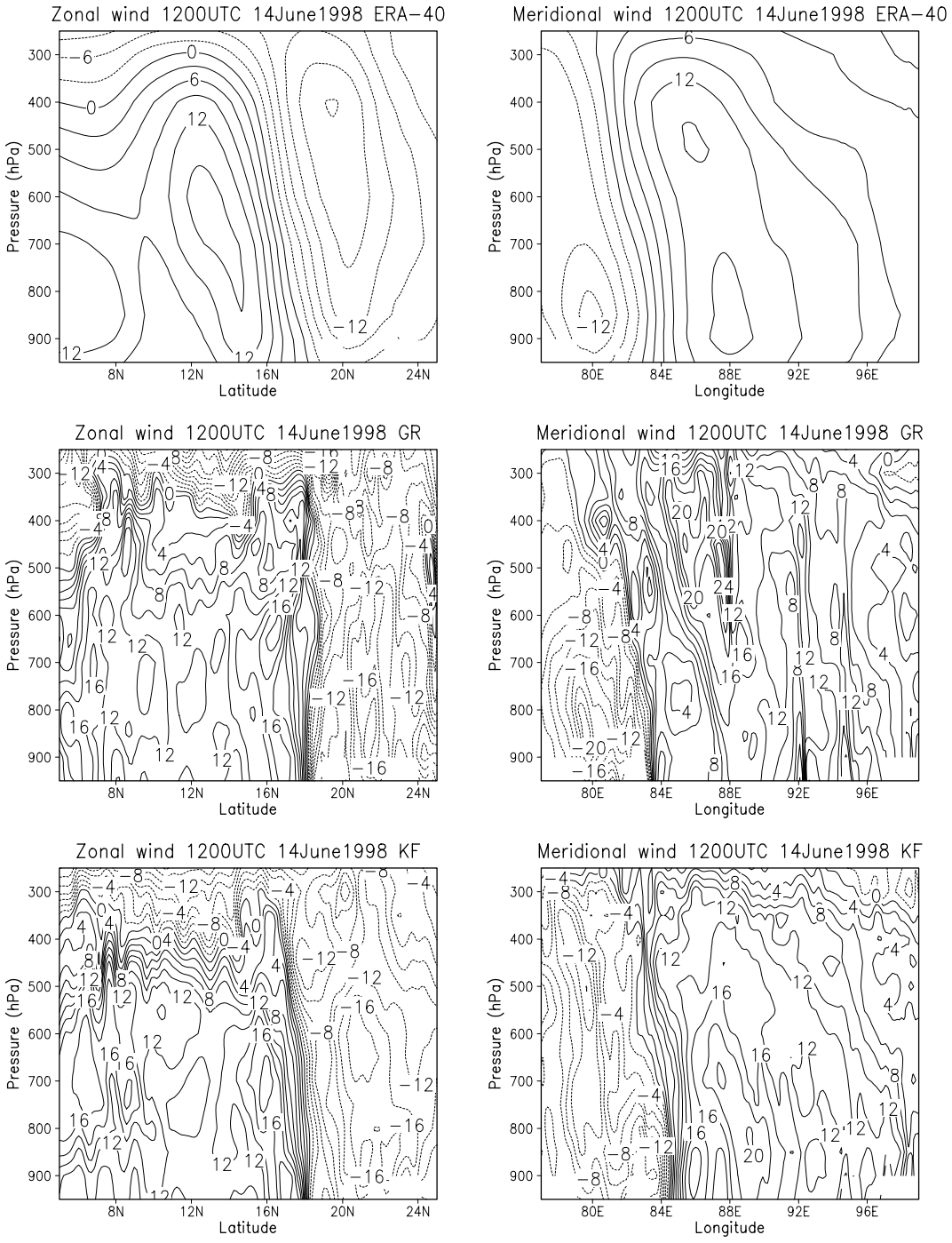

Fig. 7. Vertical cross section of the zonal and meridional wind along the centers of the depression for the 24-hour simulated and the corresponding verification analysis for Case I. Domain resolution 15 km, Input: 1200 UTC 13 June 1998. Contour interval 3 m/s for ERA-40 (Top) and 2 m/s for GR (middle) and KF (bottom) simulations

$30 \times 10^{-05}\ s^{-1}$ was seen at nearly 875 hPa. Comparing the simulated vorticity with ERA-40 reanalysis one can see that the model simulated an intense depression.

In Case II (Fig. 12), and Case III (Fig. 13) also one can see that the model simulated vorticies of stronger intensity compared to the reanalysis. In Case II, it can be seen that the GR simulated a secondary intense vortex ahead of the depression centre. This can be seen in both the 24- and 48-hours simulations. A secondary strong vortex can also be seen in the case of KF simulation but

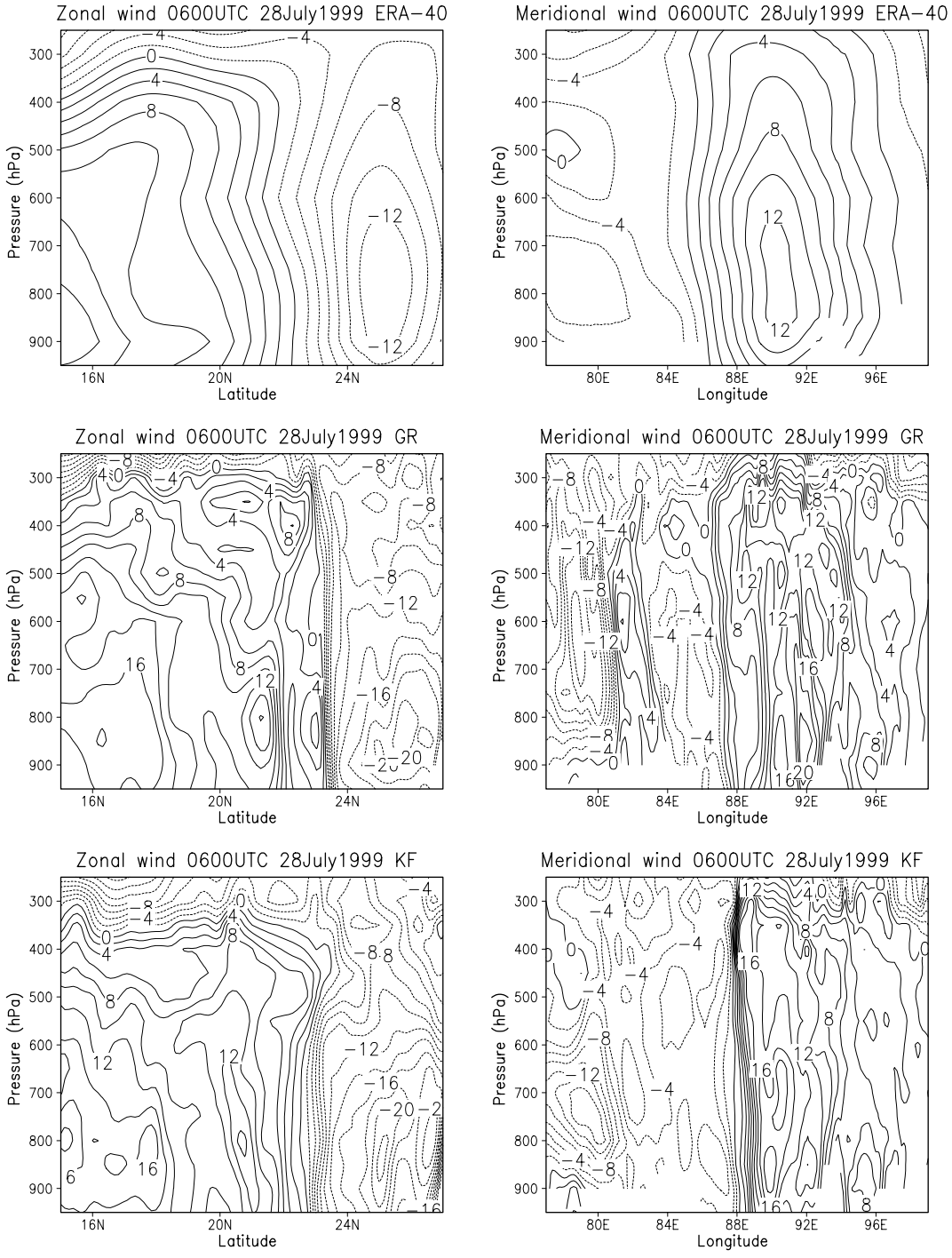

Fig. 8. Same as Fig. 7, but for Case II. Input: 0600 UTC 27 July 1999. Contour interval 2 m/s

only in the 48-hour simulation. This feature is not seen in the ERA-40 reanalysis.

3.4 Rainfall fields

The 24-hour accumulated convective, stratiform, the total rainfall simulated by the model and the observed station rainfall, for all the cases are presented in Figs. 14–16. Since the daily rainfall observations of IMD are available at 03 UTC of each day for verification, the rainfall forecasts between 15 and 39 hours of model integration have been accumulated and presented for the cases I and III, for Case II, the rainfall forecasts

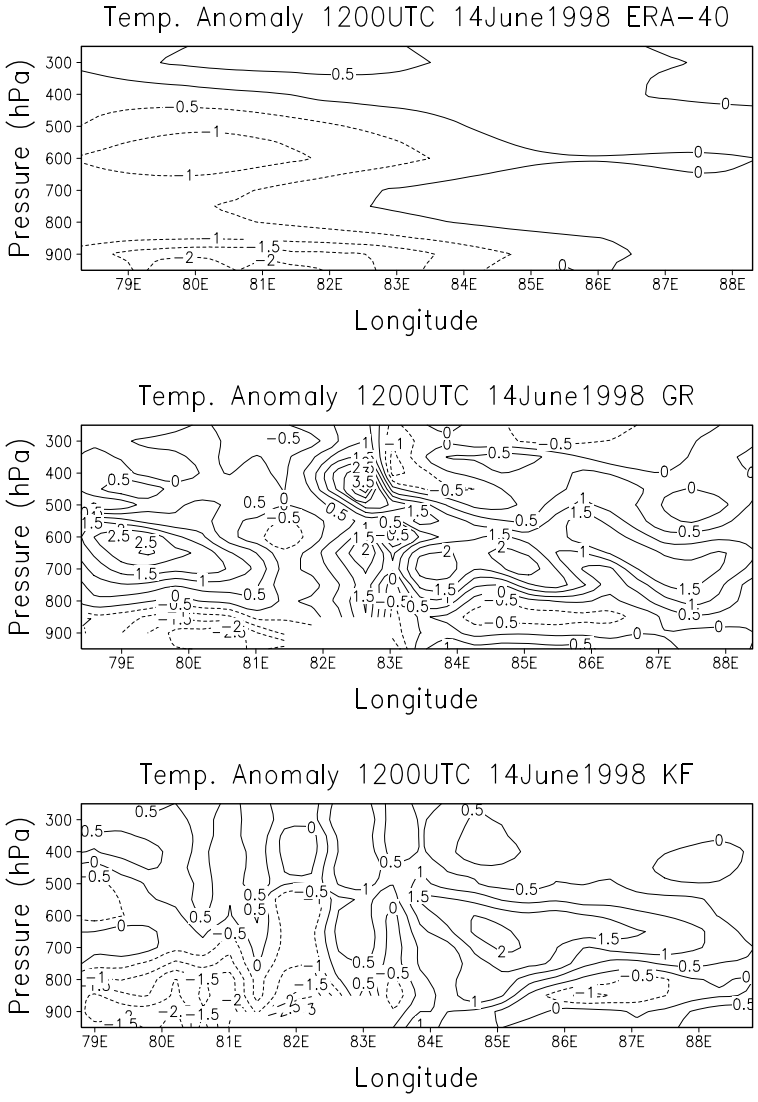

Fig. 9. Vertical cross section of the 24-hour simulated and ERA-40 latitudinal temperature anomaly (K) at the center of the depressions for Case I. Domain resolution 45 km, Input: 1200 UTC 13 June 1998. ERA-40 (Top), GR (middle) and KF (bottom)

between 21 and 45 hours of model integration have been accumulated.

For Case I, on seeing the observational data (Fig. 14e), we can see that the coastal Andhra–Orissa coast, and central India north of 15° N up to 22° N received heavy to very heavy rainfall. The maximum rainfall of 16 cm was reported at Ramagundam (18.77° N, 79.43° E). The Andhra–Orissa coast received a maximum rainfall of 4 cm and the west coast of India received very less rainfall with 3 cm and 1 cm reported at two stations. Over northern India, the rainfall is very scattered with one station reporting 5 cm of rain and most of the other stations reporting a negligible rainfall. The GR scheme, at a resolution of 15 km, predicted heavy rainfall of 15 cm at three locations one at 19.5° N, 80.9° E, the other two at 19.05° N, 81.5° E and 18.4° N, 82.2° E. The model simulated rainfalls of the order of more than 5 cm at some parts of the northern India nearer to the foot hills of Himalayas and at the west coast of India. The model also simulated very heavy rainfalls over the oceanic region. At 45 km resolution (figure not shown), the GR scheme simulated a maximum rainfall of 13 cm, 11 cm and 13 cm at the same locations as the 15 km simulation. Also, the parts of northern India and the west coast received less rainfall compared to the 15 km simulation. However, at both the resolutions, the model failed to simulate any rainfall near the Andhra–Orissa coast, where the observations showed rainfalls of the order of 4 cms. The KF scheme, at 15 km resolution, simulated a maximum rainfall of 16 cm at 18.4° N, 82.4° E. Along the Andhra–Orissa coast one can see from the figure, that the KF scheme could

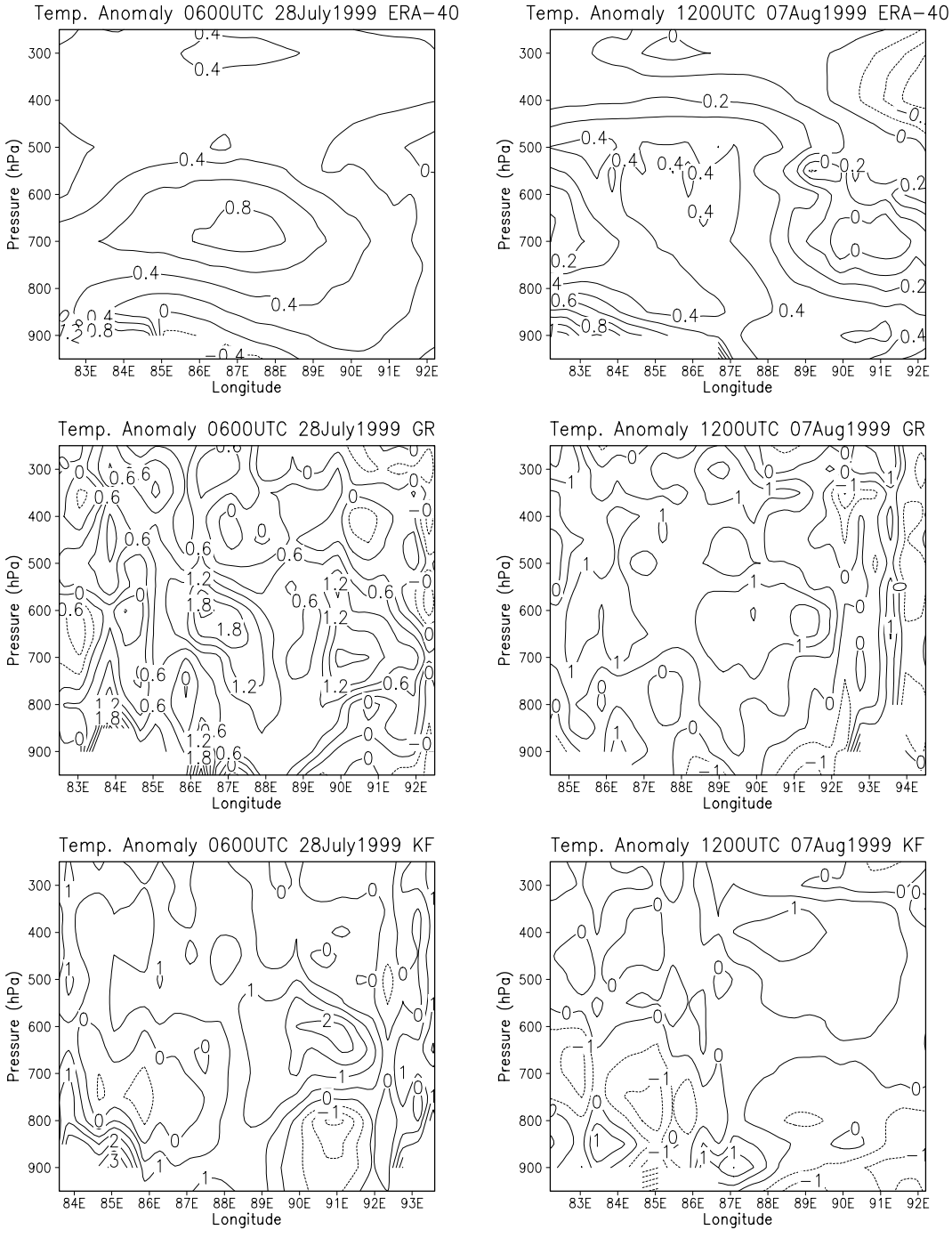

Fig. 10. Same as Fig. 9, but for Case II and Case III. Input: 0600 UTC 27 July 1999 for Case II and 1200 UTC 06 Aug. 1999 for Case III

simulate the rainfall nearer to the observed. The rainfall over the northern Indian and along the coast is also comparable to the observations. The oceanic regions also received less rainfall compared to the GR simulation. At 45 km resolution, the scheme simulated a maximum rainfall of 13 cm at the same location as the 15 km simulation. The distribution of the rainfall is similar to the 15 km simulation but with smaller magnitudes of rainfall. A look at Fig. 14b and d shows that both the schemes are able to simulate rainfall maxima in the south west quadrant of the monsoon depression. From Fig. 14a, it can be seen that the GR scheme simulates most of the

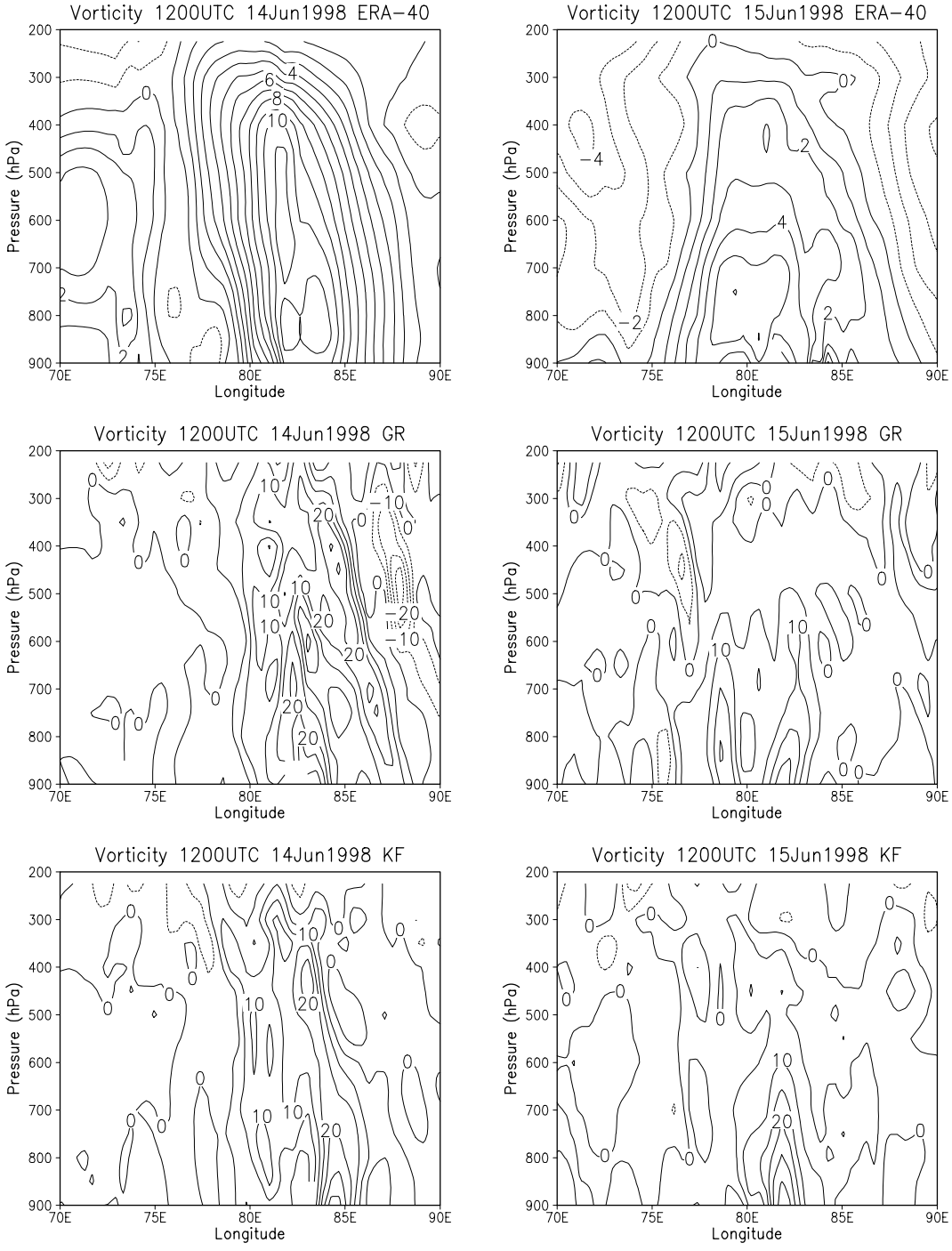

Fig. 11. Vertical cross section of the 24- and 48-hour simulated and ERA-40 vorticity ($\times 10^{-5}\,s^{-1}$) along the center of the depressions for Case I. Domain resolution 45 km, Input: 1200 UTC 13 June 1998. ERA-40 (Top), GR (middle) and KF (bottom)

rainfall due to the non-convective processes. The KF scheme (Fig. 14c) produces the rainfall in the south western quadrant mostly due to non-convective processes but the rainfall over the oceans and other parts of the land mass is dominated by convective processes. Comparing the rainfall simulated by the model with the GPCP rainfall data over the oceans (Fig. 17a) we can see that KF simulates realistic rainfall over the oceanic regions.

During the 24-hour period of 0300 UTC 28th July 1999 to 0300 UTC 29th July (Case II), the

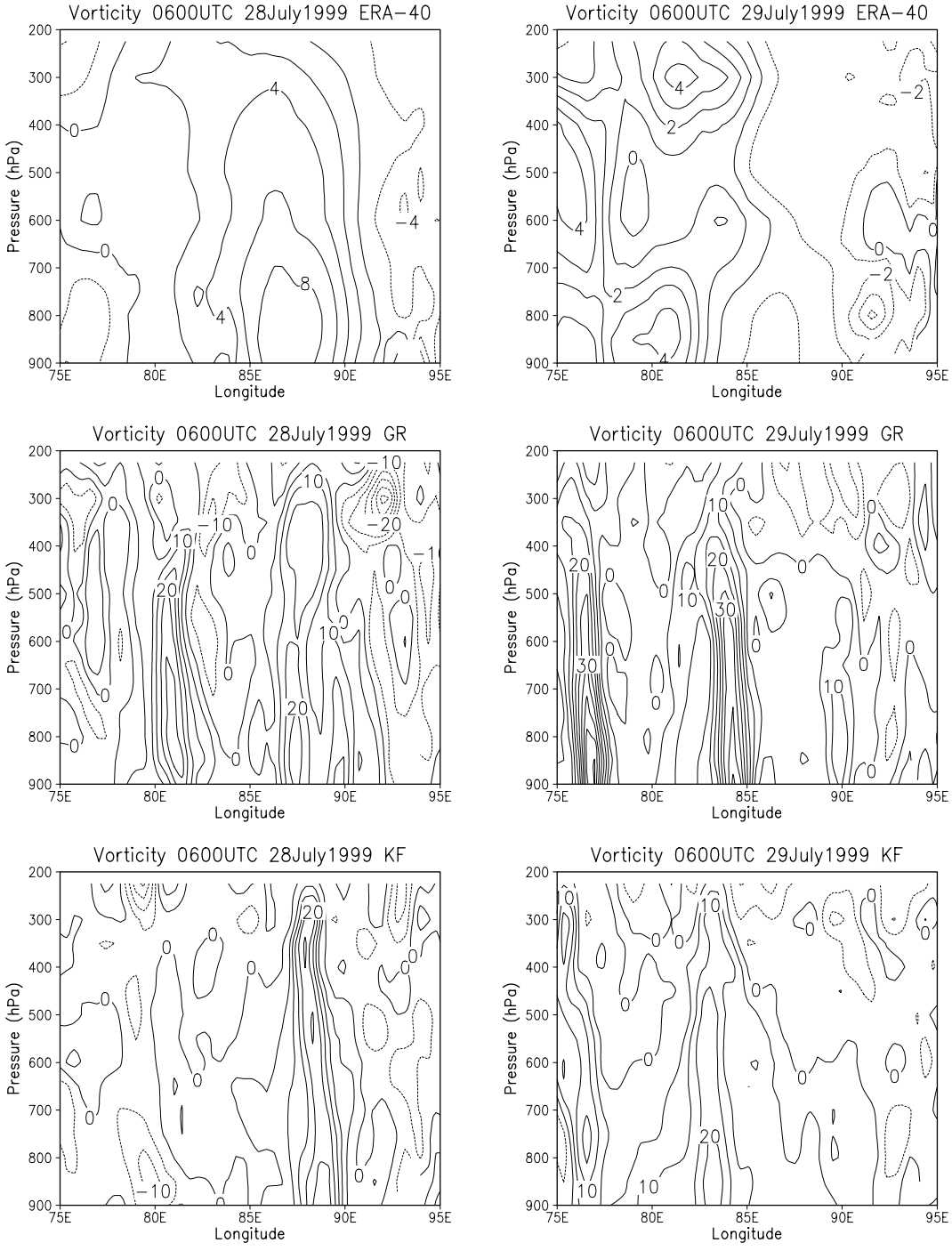

Fig. 12. Same as Fig. 11, but for Case II. Input: 0600 UTC 27 July 1999

depression moved from 23.0° N, 86.5° E, a location nearer to the West Bengal–Orissa coast, to 24.5° N, 81.0° E very close to Satna (24.57° N, 80.83° E) producing heavy to very heavy rainfall over North India. The rainfalls during the period are shown in Fig. 15. Satna recorded a rainfall of 18 cm over the 24-hour period. Gwalior (26.23° N, 78.25° E) received a rainfall of 15 cm. Along the track of the depression, a rainfall of 2–5 cms were recorded. The GR simulation for the same period and for 15 km resolution run, shows a two regions of heavy to very heavy rainfall, with maximum rainfalls of 23 cm and 21 cm at 23.25° N, 70.0° E and 23.25° N, 85° E respectively. The GR scheme simulated a heavy rainfall near the foot hills of Himalayas

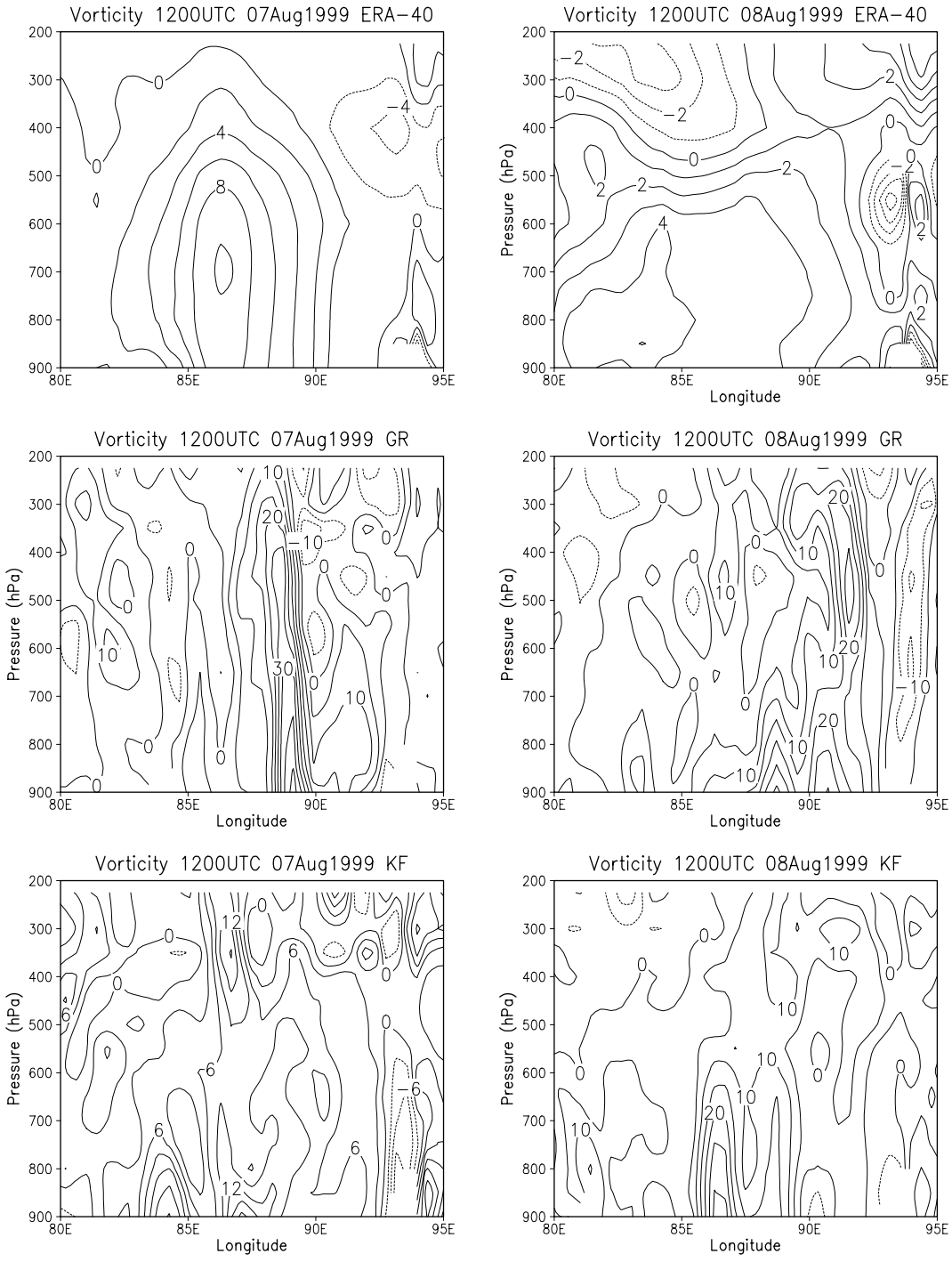

Fig. 13. Same as Fig. 11, but for Case III. Input: 1200 UTC 06 Aug. 1999

and also over the oceanic regions. The simulation at 45 km also shows the two regions of heavy rainfall with lesser magnitudes of rainfall. The KF scheme on the other hand simulated a maximum rainfall of 12 cm at 24.5° N, 80.0° E and 16 cm at 21.5° N, 85.0° E, showing that the model simulated less rainfall at the observed maximum rainfall locations. However the distribution of the rainfall over the land is similar to the observed. At 45 km resolution the model simulated less rainfall compared to the observed over the whole of the land. From Fig. 15, it can be seen that the maximum rainfall is in the south west quadrant of the depression in both the simu-

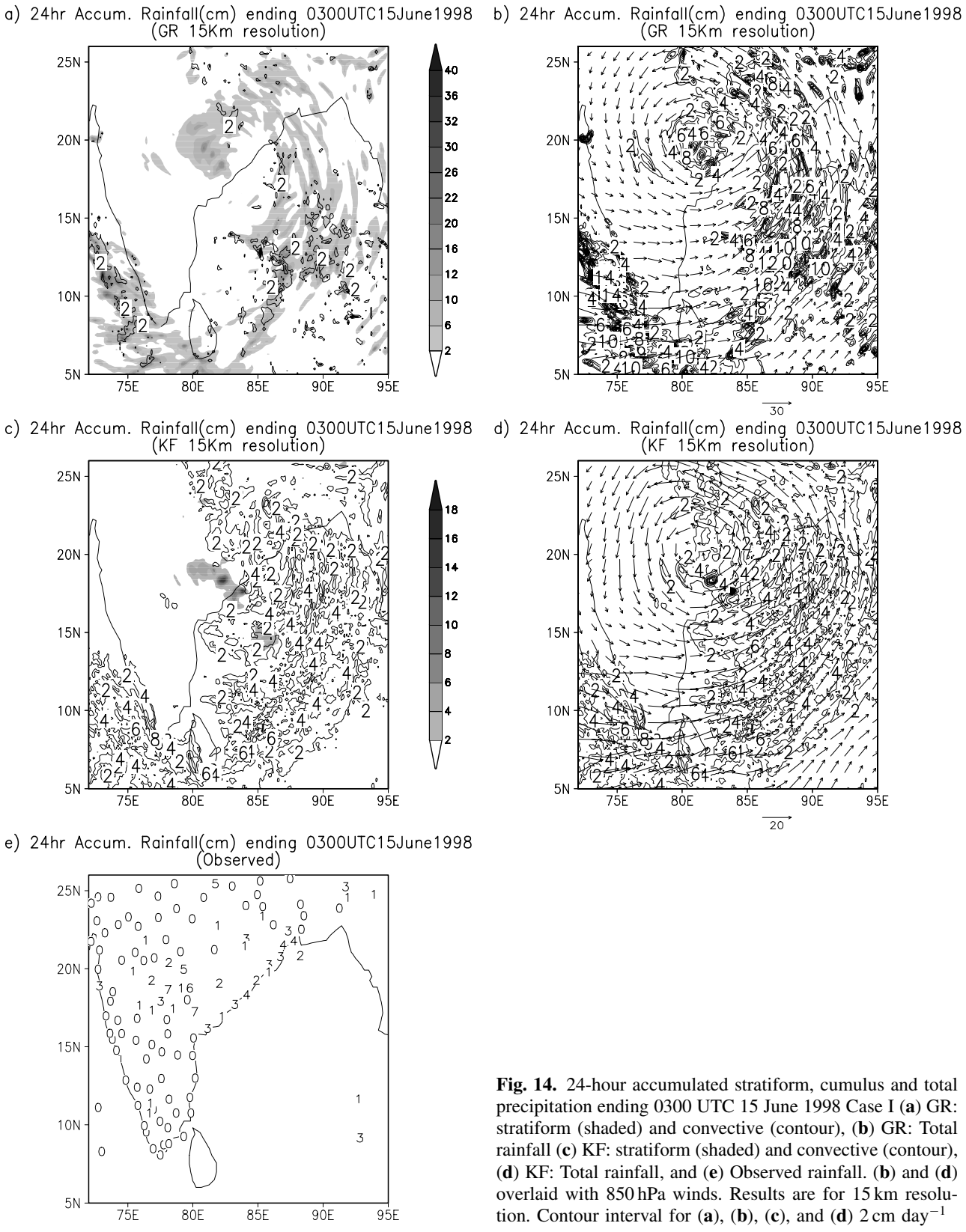

Fig. 14. 24-hour accumulated stratiform, cumulus and total precipitation ending 0300 UTC 15 June 1998 Case I (**a**) GR: stratiform (shaded) and convective (contour), (**b**) GR: Total rainfall (**c**) KF: stratiform (shaded) and convective (contour), (**d**) KF: Total rainfall, and (**e**) Observed rainfall. (**b**) and (**d**) overlaid with 850 hPa winds. Results are for 15 km resolution. Contour interval for (**a**), (**b**), (**c**), and (**d**) 2 cm day^{-1}

lations. It can also be seen that, most of the rainfall in this quadrant is due to stratiform processes. Comparing the rainfall simulation over the oceanic regions with GPCP data (Fig. 15b) we find that the rainfall over the oceanic region is more realistically simulated by KF scheme.

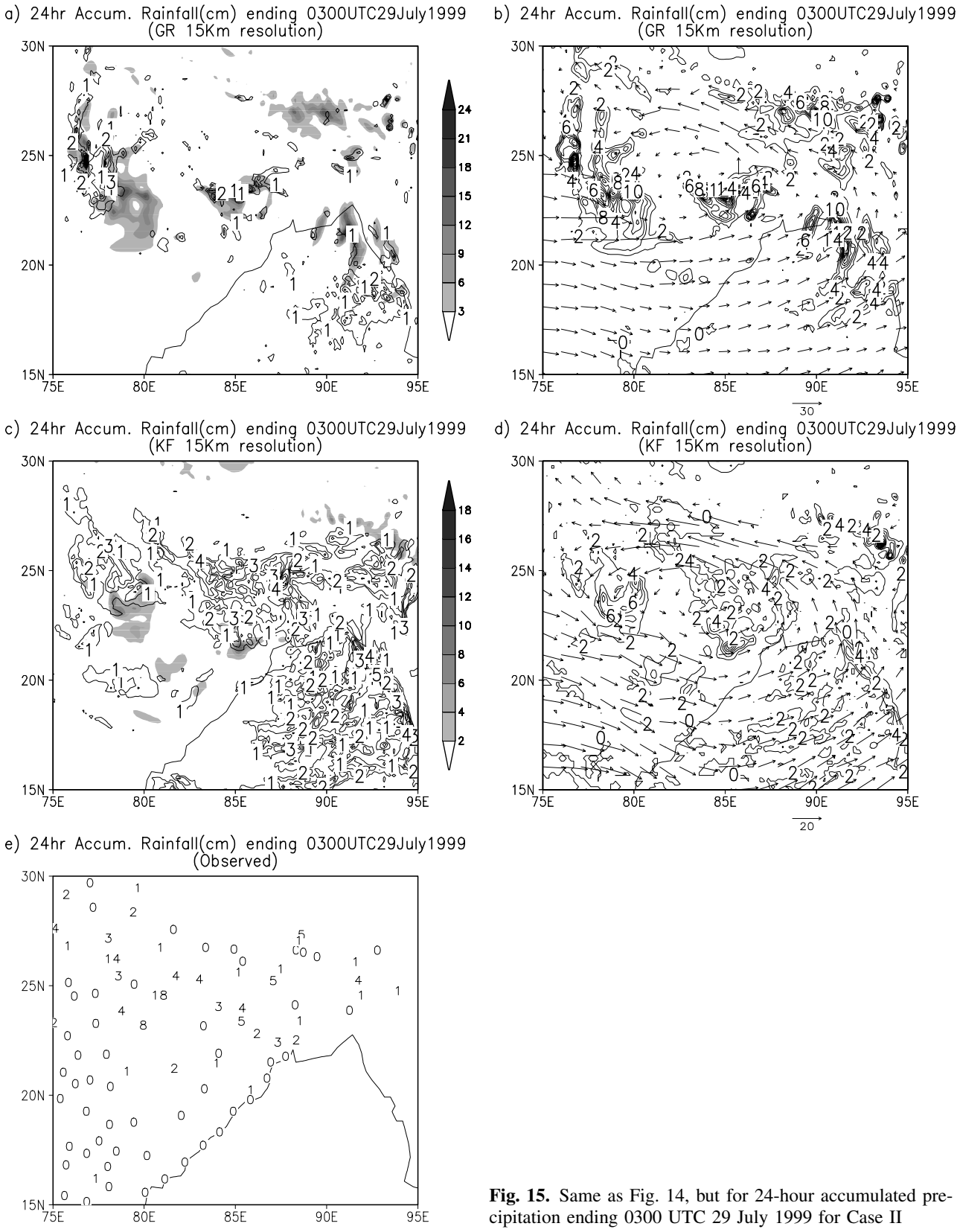

Fig. 15. Same as Fig. 14, but for 24-hour accumulated precipitation ending 0300 UTC 29 July 1999 for Case II

In Case III, one can see a maximum observed rainfall (Fig. 16e) of 15 cm at Nagpur (21.1° N, 79.05° E), 12 cm at Aurangabad (19.85° N, 75.4° E) and 10 cm at Betul (21.87° N, 77.93° E) all the stations located in Maharashtra. The depression moved from 22.5° N, 87.5° E at 0300 UTC

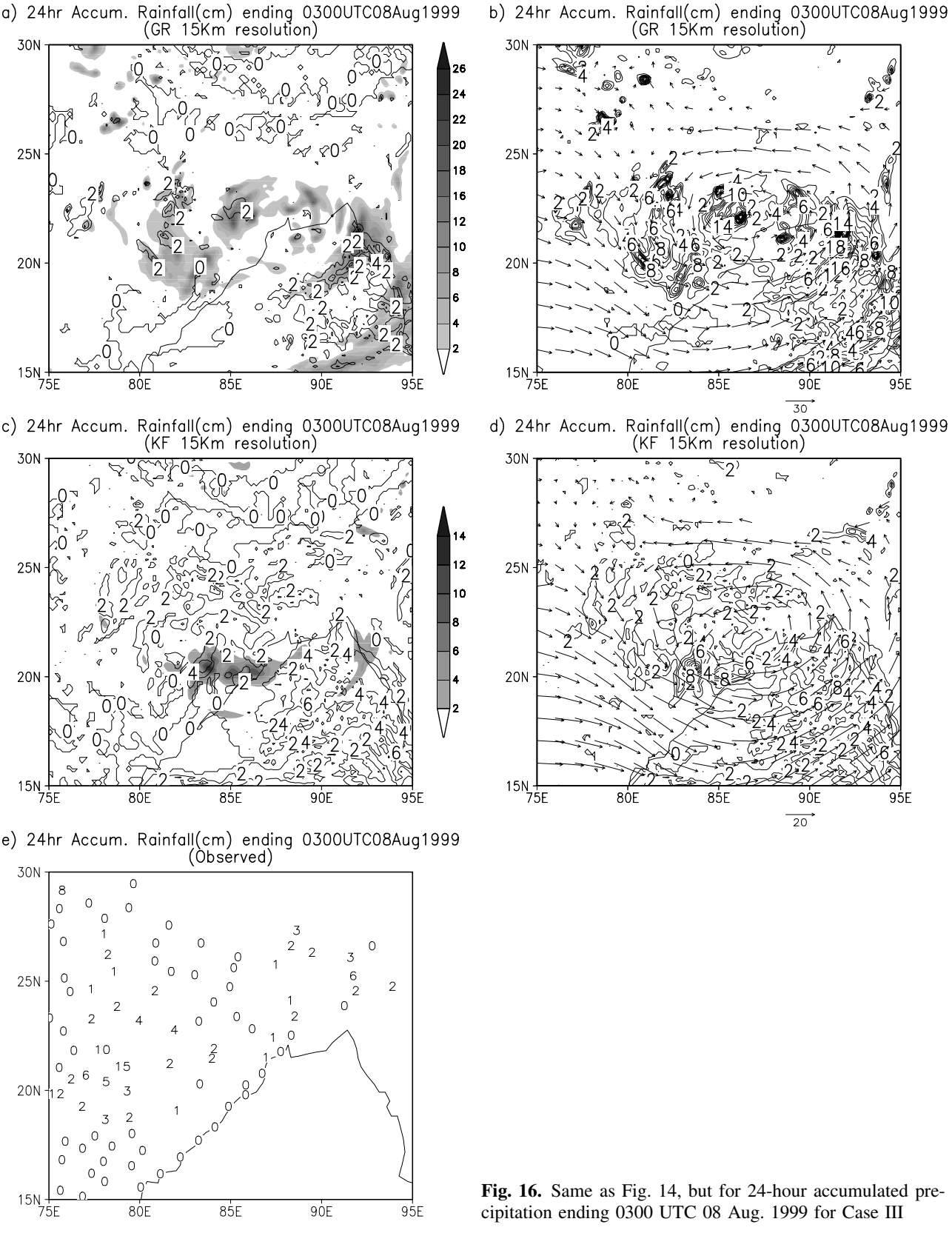

Fig. 16. Same as Fig. 14, but for 24-hour accumulated precipitation ending 0300 UTC 08 Aug. 1999 for Case III

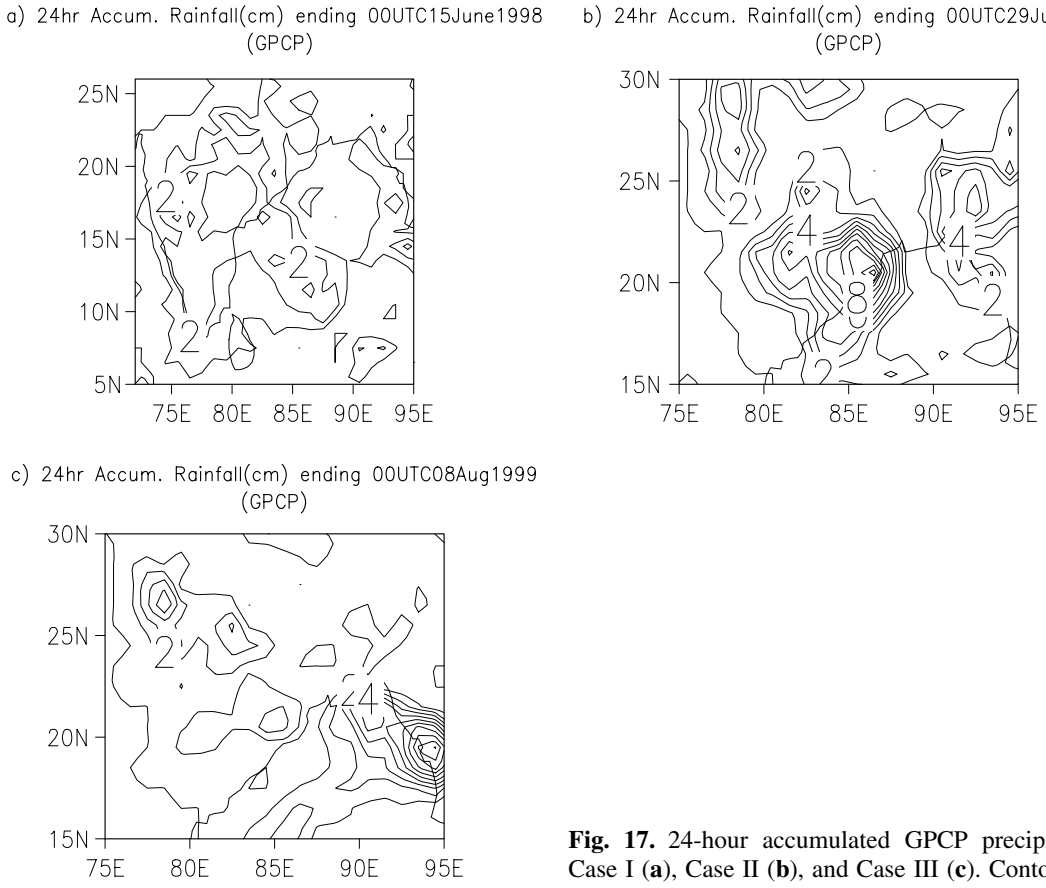

Fig. 17. 24-hour accumulated GPCP precipitation (cm day^{-1}) for Case I (**a**), Case II (**b**), and Case III (**c**). Contour interval 2 cm day^{-1}

7th August 1999 to 22.5° N 86.0° E at 0300 UTC 8th August 1999. Along its track one can see a rainfall amounts ranging from 1 cm to 4 cm. The GR scheme like in the other two cases, over predicted the rainfall amounts. A rainfall maximum of 14 cm is seen at 20.0° N, 81.0° E and also one can see very heavy rainfall of 18 cm at 22.0° N, 85.0° E. The scheme predicted almost negligible rainfall near the observed maximum rainfall station. The 45 km resolution run simulated less rainfall compared to the 15 km runs but higher than the observed values. The 15 km runs with KF scheme simulated a maximum rainfall of 16 cm at 20.5° N, 83.75° E. This scheme also simulated almost negligible rainfall near the observed maximum. Similar to the other cases, in this case also the maximum rainfall is seen in the southwest quadrant of the monsoon depression and also the maximum rainfall in this quadrant is dominated by stratiform processes. This agrees with the observations of Stano et al (2002) who found that the maximum rainfall in a depression is due to the stratiform processes. The rainfall over the oceanic regions is found to be more realistically simulated using KF scheme compared to the GPCP data (Fig. 17c).

In general, it is seen that the GR scheme over predicts rainfall in all the three cases. The KF scheme on the other hand is able to predict the rainfall comparable to the observation. Both the schemes have difficulty in predicting the maximum rainfall at the exact location. This is due to the locational error in the simulation of the depression. Earlier studies have shown that most of the rainfall occurs in the south-west sector of the monsoon depression. So, with large errors in the simulation of the position of the depression, as was seen in the analysis of MSLP, both the schemes have difficulty in simulating the rainfall maximum at the observed location.

To look at the reason for over prediction of rainfall using GR scheme, we calculated the ratio of the convective rainfall to the total rainfall over the entire period of integration. In MM5, the model precipitation is simulated by explicit methods for the grid resolvable precipitation and by the cumulus parameterization schemes for the non-resolvable precipitation. Both these

processes may be acting at a grid point at the same time (Grell et al, 1994). A reasonable partition between the two is important to simulate a realistic precipitation (Wang and Seaman, 1997). The explicit methods are usually activated when grid-scale saturation is reached. These methods usually tend to over predict rainfall in a convectively unstable atmosphere (Molinari, 1993). The cumulus parameterization schemes stabilize the atmosphere faster than the explicit methods removing the instability by transfer of heat and moisture.

To calculate the ratio of the convective rainfall to the total rainfall simulated by the model, the rainfall is averaged over the areas covering latitudes 10° N to 25° N and longitudes from 72° E to 95° E for Case I and over the area covering latitudes 15° N to 27° N and longitudes from 75° E to 95° E for Case II and Case III. These areas cover the whole track of the depression for the 48 hour period. Figure 18 shows the ratio of the convective rainfall to the total rainfall for KF and GR schemes for the 15 km model run. The ratio for the 45 km run gives exactly the same results showing that the schemes are insensitive to the grid resolution, in agreement with the results of Wang and Seaman (1997). From the figure, it can be seen that for all the cases, during the entire model integration, the model with the KF scheme, simulated rainfall mostly due to convective processes, though its ratio varied with time. Where as the model with the GR scheme simulated most of the rainfall due to the explicit processes. The model starts with convective precipitation due to GR but by 12 hour period the explicit processes take over, showing that the GR scheme is not convectively active in any of the cases. Wang and Seaman (1997) reported similar results in their simulations of cold and warm season events. They attributed this behavior of GR scheme to the precipitation efficiency parameter in the scheme being too small. The dominance of the explicit methods in the model with GR scheme, may also be the cause of the spurious cyclonic circulation seen in the 850 hPa wind field in Case II around the region of 24° N, 81° E on 28th July 1999 and also seen in the vertical cross section of the meridional wind field.

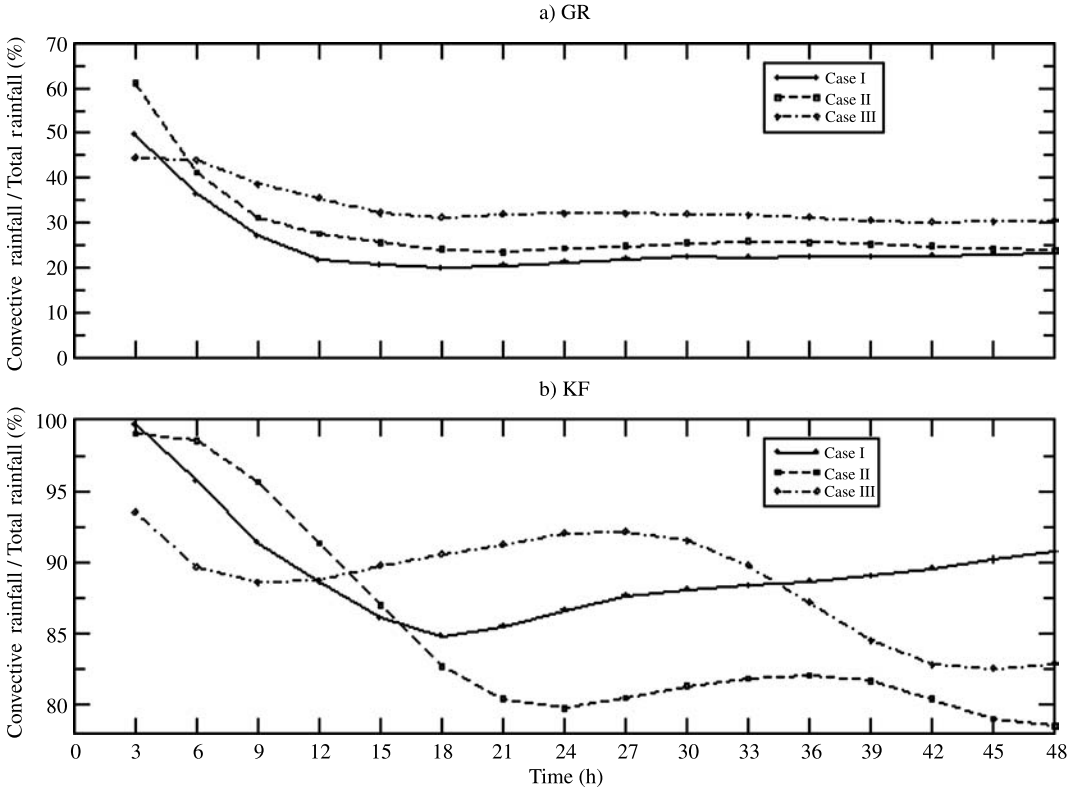

Fig. 18. Area averaged 3 hourly time series showing the ratio of convective precipitation to the total precipitation (%) for (**a**) GR and (**b**) KF for all the cases. Area Average for Case I: 10° N–25° N, 72° E–95° E, Case II and Case III: 15° N–27° N, 75° E–95° E

3.5 Apparent heat source and moisture sink

The effects of the transfer of the heat and moisture by the cumulus clouds on the large scale parameters can be estimated by calculating the apparent heat source (Q1) and apparent moisture sink (Q2) as defined by Yanai et al (1973). Using the standard equations of Yanai et al (1973; Eqs. (8) and (9)), we calculated Q1 and Q2 using the model output and the ERA-40 data interpolated to the model grid. For calculating the time derivative of the dry static energy and the mixing ratio of water vapor, we applied forward time differencing scheme to the model output at an interval of 12 hours. The area averages were computed over the same area as the ratio of the convective rainfall to the total rainfall were calculated. Figure 19 shows the vertical profiles of Q1 and Q2 for all the cases. The model simulated heating due to radiation tendency (Qr) is also plotted for all the cases. From Fig. 19, it can be seen that in Case I and Case III, the KF and GR simulate Q1 comparable to the ERA-40 analysis. Both the KF and GR simulate maximum apparent heat source at 400 hPa. The heating is due to the release of latent heat in the cumulus clouds and its upward transfer by eddies (Yanai et al, 1973). In Case II, the KF and GR simulated Q1 higher than ERA-40 analysis, with GR simulating higher that KF. This may be due to the secondary vortex seen in the KF and GR simulations (Fig. 12). The KF scheme simulated a low level moisture sink in all the cases, with maximum drying at around 800 hPa and with a secondary peak at around 400 hPa, the level corresponding to the level of maximum apparent heating. The GR scheme on the other hand has multiple peaks. The drying is usually attributed to strong down-

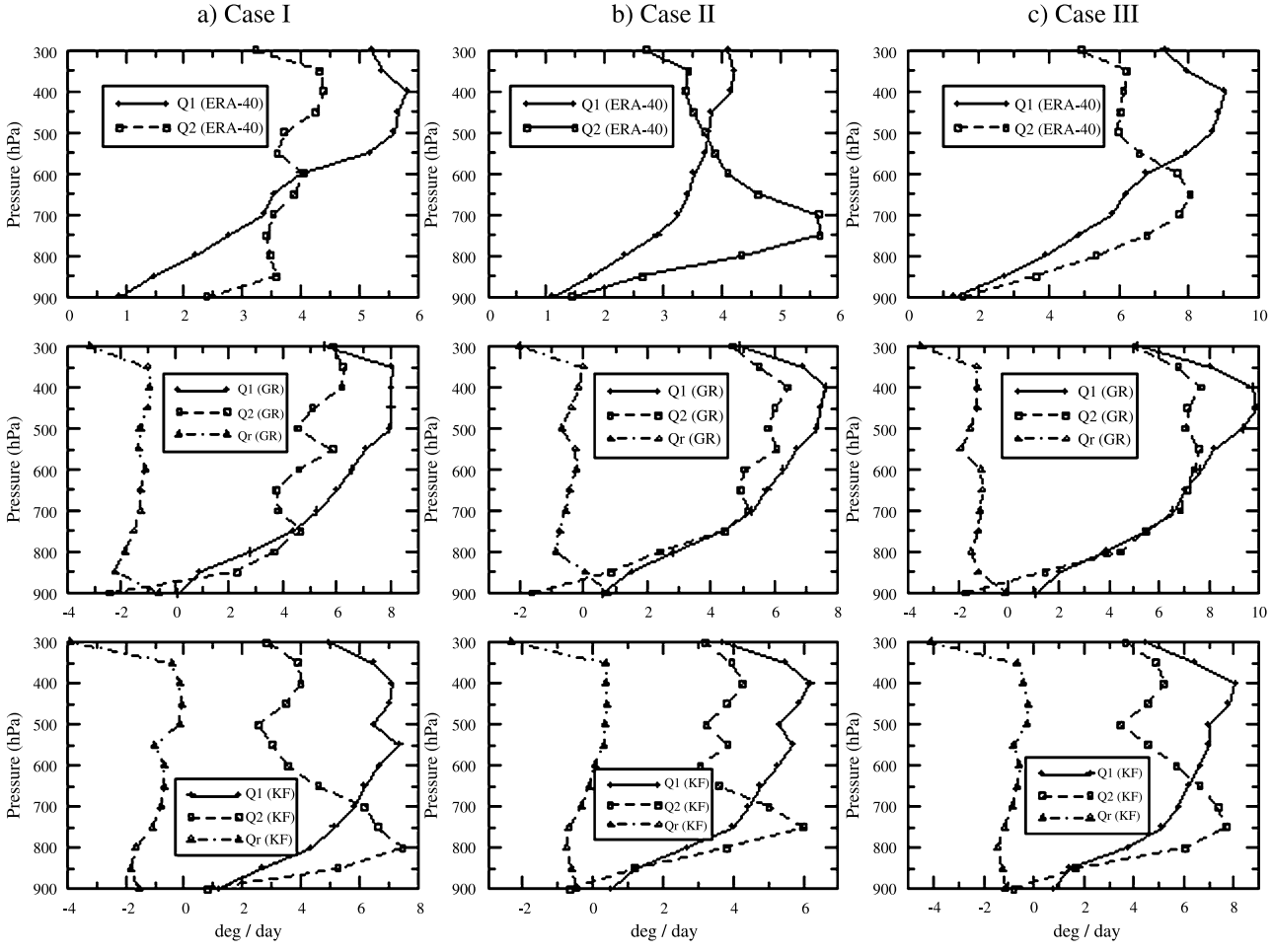

Fig. 19. 48-hour time averaged vertical profiles of area averaged Q1, Q2 and Qr for (**a**) Case I, (**b**) Case II, and (**c**) Case III for ERA-40 (top), the model simulations with GR (middle) and KF (bottom). Area average for Case I: 10° N–25° N, 72° E–95° E, Case II and Case III: 15° N–27° N, 75° E–95° E

Table 3a. RMS error of the mean sea-level pressure

	Mean sea-level pressure (hPa)	
	24 h	48 h
Case I		
GR	2.36	3.97
KF	1.41	2.3
Case II		
GR	2.32	2.09
KF	2.07	1.45
Case III		
GR	2.84	2.86
KF	2.48	1.59

drafts (Krishnamurti et al, 1983). The GR and KF schemes show a moisture cooling in the lower levels, below 875 hPa in Case II and Case III. This may be due the dominance of re evaporation of the droplets because of strong winds associated with the intense depressions simulated by the schemes. The cooling is also observed in Case I of GR simulation. The ERA-40 data shows a maximum apparent heating at 400 hPa and maximum drying at around 850 hPa in Case I, 750 hPa in Case II and 650 hPa in Case III. From the figure, it can be seen that the profiles of Q1 and Q2 simulated by the model with KF are comparable to ERA-40 than the profiles simulated by the model with GR scheme.

Table 3b. RMS error of zonal and meridional wind at 850 hPa, 700 hPa, 500 hPa and 200 hPa levels simulated by the model

	Zonal wind (m/s)								Meridional wind (m/s)							
	850 hPa		700 hPa		500 hPa		200 hPa		850 hPa		700 hPa		500 hPa		200 hPa	
	24 h	48 h	24 h	48 h	24 h	48 h	24 h	48 h	24 h	48 h	24 h	48 h	24 h	48 h	24 h	48 h
Case I																
GR	3.66	5.93	3.91	6.11	5.32	5.3	7.1	3.91	3.6	3.17	3.77	3.93	4.07	4.06	6.02	3.8
KF	3.4	5.36	4.03	4.96	3.97	3.52	4.7	4.81	4.07	3.54	2.83	2.78	3.21	4.65	5.2	3.63
Case II																
GR	3.9	5.4	3.55	2.81	3.49	2.34	5.74	4.69	2.93	3.82	3.18	3.68	3.27	4.54	5.35	4.56
KF	3.41	4.93	3.11	3.83	3.27	2.7	5.16	2.56	2.83	1.9	2.98	3.09	3.13	5.44	4.85	4.09
Case III																
GR	3.58	6.58	3.58	5.52	3.81	2.97	5.24	4.28	3.32	3.36	3.43	3.09	3.64	3.77	4.2	4.85
KF	2.92	5.28	2.68	3.93	3.61	2.62	4.21	3.78	3.25	2.6	3.06	3.89	3.18	3.85	4.22	3.37

Table 3c. Same as Table 3b, but for geopotential height and temperature

	Geopotential height (m)								Temperature (K)							
	850 hPa		700 hPa		500 hPa		200 hPa		850 hPa		700 hPa		500 hPa		200 hPa	
	24 h	48 h	24 h	48 h	24 h	48 h	24 h	48 h	24 h	48 h	24 h	48 h	24 h	48 h	24 h	48 h
Case I																
GR	10.1	11.3	11.6	18.1	11.4	22.3	27.5	15.2	1.78	3.91	1.51	2.4	1.16	0.93	1.76	0.86
KF	13.6	21.5	12.6	24.9	9.8	18	28.3	22.8	1.17	3.01	0.95	1.08	0.83	1.34	0.53	0.62
Case II																
GR	14.2	16.7	19	18.4	19.2	14.1	27	12.9	1.75	1.51	1.4	1.1	1.62	1.57	1.62	0.92
KF	17.3	21.5	20	21.9	18.4	13.2	28.1	16.4	1.2	0.85	1.11	0.75	1.77	1.21	1.34	0.58
Case III																
GR	9.6	10.4	11.9	14.2	18.8	21	26.1	14.1	1.25	1.91	1.26	1.8	1.53	0.95	1.27	0.92
KF	11.2	14.5	12.2	16.7	17.7	17.4	26.6	15.2	1.15	1.06	1.04	1.02	1.56	1.06	1.23	0.74

The net radiational heating Qr is seen to be negative throughout the atmosphere in both the simulations. Both the schemes simulated a net radiational cooling of 1–2°/day, which is comparable to Qr obtained by Yanai et al (1973).

3.6 Root mean square error of the simulations

As is well known, the regional models are used to improve the GCM simulations by adding regional components to it without deviating much from the GCM simulation. The calculation of Root Mean Square Error (RMSE) helps in examining the deviation of the regional model from the driving GCM, in this case from the ERA-40 data. The computed values of RMSE for MSLP, zonal wind, meridional wind geopotential height and temperature at 850 hPa, 700 hPa, 500 hPa and 200 hPa levels along with the RMSE in MSLP, for the entire domain of the 15 km resolution model run are shown in Table 3a–c. For 45 km resolution similar results were obtained. The tabulated values show that the large-scale fields are well simulated by both the schemes for all the cases. From Table 3a, it can be seen that the errors in the simulation of MSLP are greater with GR scheme than with KF scheme. For Case II and Case III, the 48-hour errors are found to be less than the 24 hour errors in the KF simulation. These results indicate that the MSLP distribution in the KF simulation are nearer to the ERA-40 distribution, even though there are large differences in the central pressures and its location (Table 2). From Table 3b and c, one can see that the errors in GR scheme are considerable larger than KF for temperature, zonal wind and meridional wind at all the levels. However GR simulated geopotential height better than the KF scheme. From the table it can also be seen that the errors in the 48-hour fields of temperature and meridional wind are less than the 24 hour errors at all levels in the KF simulation for Case II and Case III.

4. Conclusions

In this study, we investigated the sensitivity of the simulation of monsoon depressions in MM5 using two different cumulus parameterization schemes GR and KF. Three cases of monsoon depressions which formed in Bay of Bengal during 1998 and 1999 were considered for the study. The six hourly ERA-40 data was used to provide the initial and lateral boundary conditions to the model.

The results show that both the schemes are able to simulate the broad features of the monsoon depression comparable to the ERA-40 data. The KF scheme simulated a deeper depression compared to the analysis but the pressure distribution across the peninsula and oceans was similar to the analysis. The GR scheme could simulate the central pressures comparable to the analysis but simulated higher pressures over the rest of the domain. The winds of higher magnitudes were simulated by both the schemes. The GR scheme simulated a spurious cyclonic circulation in one of the cases.

Both the schemes had difficulty in simulating the maximum rainfall at the observed locations. However the distribution of the rainfall was comparable to the observations in the KF simulation. The GR simulated higher rainfall. On calculating the ratio of the convective rainfall to the total rainfall simulated by the model, it is seen that the KF simulated most of the rainfall through convective processes whereas the explicit rainfall processes were dominant in the model with GR scheme. Marked improvement in the rainfall was seen in the model runs with 15 km resolution compared to the 45 resolution runs. Both the schemes could simulate the maximum rainfall in the south-west sector of the depressions. Computation of the vertical profiles of Q1 and Q2 showed that both the schemes simulated Q1 maxima at 400 hPa comparable to the ERA-40. The simulation of Q2 by KF is more comparable to the verifying analysis. The RMSE calculations show the KF to follow the driving ERA-40 data more closely than the GR simulations.

From the study it is seen that the simulation of the monsoon depression are sensitive to the choice of the cumulus parameterization schemes in MM5. Though both the schemes could simulate the large scale features well, both had difficulties in the prediction of the rainfall. We are carrying out further studies to test the sensitivity of the simulation of the depressions to the tuning parameters in the cumulus schemes for many cases of depressions. This will help in better understanding the cumulus parameterizations required for the simulation of the depressions and in improving their simulations using MM5.

Acknowledgments

The ERA-40 data was obtained from European Center for Medium Range Forecast Center (ECMWF) through their web site *http://www.ecmwf.int.* The authors wish to thank ECMWF for the data. The authors also wish to thank the Computing Services of the University College Dublin for providing the computing facilities for carrying out the simulations. We also thank two anonymous reviewers for their insightful comments on this paper.

References

Arakawa A, Schubert WH (1974) Interaction of a cumulus cloud ensemble with the large scale environment, Part I. J Atmos Sci 31: 674–701

Bhowmik SK (2003) Prediction of monsoon rainfall with a nested grid mesoscale limited area model. Proc Indian Acad Sci (Earth Planet Sci) 112: 499–519

Bougeault P, Mascart P (2001) The Meso-NH Atmospheric Simulation System: Scientific documentation. Published by METEO France and CNRS 337 pp. Available from http://www.aero.obs-mip.fr/mesonh/

Chen TC, Yoon JH (2000) Some remarks on the westward propagation of the monsoon depression. Tellus 52A: 487–499

Daggupaty S, Sikka DR (1977) On the vorticity budget and vertical velocity distribution associated with the life cycle of a monsoon depression. J Atmos Sci 34: 773–792

Dudhia J (1996) A multi-layer soil temperature model for MM5. Preprints 6th Annual MM5 Users Workshop, Boulder, Colorado.

Dudhia J, Gill D, Manning K, Wang W, Bruyere C (2005) PSU/NCAR Mesoscale Modeling System Tutorial Class Notes and Users Guide (MM5 Modeling System Version 3). Online publication available from http://www.mmm.ucar.edu/mm5/documents/tutorial-v3-notes.html

Godbole RV (1977) The composite structure of the monsoon depression. Tellus 29: 25–40

Grell G, Dudhia J, Stauffe D (1994) A description of the Fifth-generation Penn State/NCAR Mesoscale Model (MM5). NCAR Tech. Note, NCAR/TN-398 + STR. 138pp

Hong SY, Pan HL (1996) Nonlocal boundary layer vertical diffusion in a medium-range forecast model. Mon Wea Rev 122: 927–945

Kain JS, Fritsch JM (1993) Convective parameterization for mesoscale models: The Kain-Fritsch scheme. The representation of Cumulus convection in numerical models. Meteor Monogr Amer Met Soc 46: 165–170

Krishnamurti TN, Kanamitsu M, Godbole RV, Chang C, Carr F, Chow JH (1975) Study of a monsoon depression (I). Synoptic structure. J Meteror Soc Japan 53: 227–239

Krishnamurti TN, Simon LN, Pasch R (1983) Cumulus parameterization and rainfall rates II. Mon Wea Rev 111: 815–828

Manabe S (1969) Climate and the ocean circulations, 1. The atmospheric circulation and the hydrology of the Earth's surface. Mon Wea Rev 97: 739–774

Molinari J (1993) An overview of cumulus parameterization in mesoscale models. The representation of Cumulus convection in numerical models. Meteor Monogr Amer Met Soc 46: 155–158

Potty KVJ, Mohanty UC, Raman S (2000) Numerical simulation of monsoon depressions over India with high-resolution nested regional model. Meteor Appl 7: 45–60

Sikka DR (1977) Some aspects of the life history, structure and movement of the depressions. Pure Appl Geophys 115: 1501–1529

Stano G, Krishnamurti TN, Kumar TSVV, Chakaborty A (2002) Hydrometeor structure of a composite monsoon depression using the TRMM radar. Tellus 54A: 370–381

Thapliyal V, Desai DS, Krishnan V (1999) Cyclones and depressions over north Indian Ocean during 1998. Mausam 50: 233–242

Thapliyal V, Desai DS, Krishnan V (2000) Cyclones and depressions over north Indian Ocean during 1999. Mausam 51: 215–224

Vaidya SS, Singh SS (1997) Thermodynamic adjustment parameters in the Betts-Miller scheme of convection. Wea Forecast 12: 819–825

Vaidya SS, Singh SS (2000) Applying the Betts-Miller-Janjic scheme of convection in prediction of the Indian monsoon. Wea Forecast 15: 349–356

Vaidya SS, Mukopadhyay P, Trivedi DK, Sanjay J, Singh SS (2004) Prediction of tropical systems over Indian region using mesoscale model. Meteorol Atmos Phys 86: 63–72

Wang W, Seaman NL (1997) A Comparison study of convective parameterization schemes in a mesoscale model. Mon Wea Rev 125: 252–278

Yanai M, Esbensen S, Chu JH (1973) Determination of bulk properties of tropical cloud clusters from large-scale heat and moisture budgets. J Atmos Sci 30: 611–627

Corresponding author's address: J. Venkata Ratnam, Department of Mathematical Physics, University College Dublin, Belfield, Dublin, Ireland 4 (E-mail: jvratnam@cdac.in; venkata.jayanthi@ucd.ie)